



TALLINNA TEHNIKAÜLIKOOL
TALLINN UNIVERSITY OF TECHNOLOGY

Department of Materials and Environmental
Technology

GROWTH OF $\text{Cu}_2\text{CdGeSe}_4$ MONOGRAIN POWDERS IN
MOLTEN SALTS

$\text{Cu}_2\text{CdGeSe}_4$ MONOTERAPULBRITE SÜNTEES SULADES SOOLADES

MASTER THESIS

Student: Xiaofeng Li
/name/
Student code: 165549KAYM
Supervisor: Dr. Marit Kauk-Kuusik
Senior Research Scientist
/name, position/

Tallinn, 2018

AUTHOR'S DECLARATION

Hereby I declare, that I have written this thesis independently.

No academic degree has been applied for based on this material. All works, major viewpoints and data of the other authors used in this thesis have been referenced.

"....." 201.....

Author:

/signature /

Thesis is in accordance with terms and requirements

"....." 201.....

Supervisor:

/signature/

Accepted for defence

"....."201... .

Chairman of theses defence commission:

/name and signature/

THESIS TASK

Student: Xiaofeng Li, 165549KAYM (name, student code)

Study programme, KAYM, Materials and Processes of Sustainable Energetics (code and title)

main speciality: Processes of Sustainable Energetics

Supervisor(s): Senior Research Scientist, Marit Kauk-Kuusik, +372 620 3360
(position, name, phone)

Consultants:(name, position)

..... (company, phone, e-mail)

Thesis topic:

(in English) Growth of Cu₂CdGeSe₄ monograin powders in molten salts

(in Estonian) Cu₂CdGeSe₄ monoterapulbrite süntees sulades soolades

Thesis main objectives:

1. to study the growth of Cu₂CdGeSe₄ monograin powders in molten flux materials
2. to characterize the morphology, compositional, structural and electrical properties of Cu₂CdGeSe₄ powders
3. to use synthesised powders as absorber materials in monograin layer solar cells

Thesis tasks and time schedule:

No	Task description	Deadline
1.	Selecting the preparation conditions for the synthesis of Cu ₂ CdGeSe ₄ monograin powders in the liquid phase of molten salts. Two flux materials - KI and CdI ₂ were chosen.	27.10.2017
2.	Analysing the morphology (SEM, optical microscope), crystal size distribution (sieving analysis), phase (XRD, Raman) and elemental composition (EDX) of powder depending on the synthesis temperature, time and the nature of flux material. Selecting the powders with suitable properties for monograin layer solar cells as absorber materials and characterization of devices.	22.01.2018
3.	Writting the thesis.	25.05.2018

Language: English **Deadline for submission of thesis:** "....."2018 a

Student: Xiaofeng Li "....."2018 a

/signature/

Supervisor: Dr. Marit Kauk-Kuusik "....."2018a

/signature/

Consultant: "....."201....a

/signature/

Terms of thesis closed defence and/or restricted access conditions to be formulated on the reverse side

CONTENTS

PREFACE.....	6
List of abbreviations and symbols.....	7
INTRODUCTION.....	8
1. LITERATURE REVIEW AND THE OBJECTIVE OF STUDY.....	9
1.1 Principles of solar cell.....	9
1.1.1 Review of solar cell absorber materials.....	10
1.2 Material properties of $\text{Cu}_2\text{CdGeSe}_4$	13
1.2.1 Crystal structure of $\text{Cu}_2\text{CdGeSe}_4$	13
1.2.2 Synthesis methods of $\text{Cu}_2\text{CdGeSe}_4$	14
1.2.3 The phase relations in the Cu_2Se - CdSe - GeSe_2 system.....	15
1.2.3.1 Cu_2Se - CdSe quasi-binary system.....	16
1.2.3.2 The Cu_2Se - GeSe_2 system.....	16
1.2.3.3 The CdSe - GeSe_2 system.....	17
1.2.3.4 The Cu_2GeSe_3 - CdSe system.....	17
1.2.4 Optical and electrical properties of $\text{Cu}_2\text{CdGeSe}_4$	18
1.3 Monograin powder technology.....	19
1.3.1 Overview of monograin technology.....	19
1.3.2 Monograin powder growth.....	19
1.3.2.1 Flux materials.....	20
1.3.3 Monograin layer solar cell.....	20
1.4 Summary of literature overview and the objective of the study.....	21
2. EXPERIMENTAL.....	23
2.1 Preparation of monograins.....	23
2.1.1 Post-treatment of $\text{Cu}_2\text{CdGeSe}_4$ monograin powders.....	24
2.2 Characterization of monograins.....	25
2.2.1 Particle size determination method.....	25
2.2.2 Raman spectroscopy.....	26
2.2.3 XRD analysis.....	26
2.2.4 Scanning electron microscopy (SEM).....	26
2.2.5 Energy dispersive X-ray spectroscopy (EDX).....	27
2.2.6 Grain resistance measurements.....	27
2.3 Solar cell characteristics.....	28

2.3.1 Current-Voltage measurements.....	28
2.3.2 Quantum efficiency measurements.....	28
3. RESULTS AND DISCUSSIONS.....	29
3.1 Particle size distribution.....	29
3.2 Morphology of $\text{Cu}_2\text{CdGeSe}_4$ monograin powders.....	30
3.2.1 Shape analysis by optical microscopy.....	30
3.2.2 Morphology analysis by scanning electron microscopy (SEM).....	31
3.2.2.1 Influence of chemical etching on the crystal surface morphology.....	33
3.3 Elemental composition of $\text{Cu}_2\text{CdGeSe}_4$ monograin powders.....	33
3.4 Phase composition of $\text{Cu}_2\text{CdGeSe}_4$ monograin powders.....	35
3.4.1 XRD analysis.....	35
3.4.2 Raman analysis.....	35
3.5 Electrical properties of $\text{Cu}_2\text{CdGeSe}_4$ monograin powders.....	37
3.6 Device characterization.....	37
SUMMARY.....	39
LIST OF REFERENCES.....	40
APPENDIX.....	44

PREFACE

The topic of this thesis was initiated by my supervisor, senior research scientist Dr. Marit Kauk-Kuusik. The thesis is based on the experimental work carried out in the Laboratory of Photovoltaic Materials at the Department of Materials and Environmental Technology, Tallinn University of Technology (TUT).

First, I'd like to show my biggest thank to my supervisor, senior research scientist Dr. Marit Kauk-Kuusik, she always give me lots of suggestions patiently in both of my experimental and my thesis work. Second, I'd like to thank my research group members Dr. Kristi Timmo, Dr. Maris Pilvet, Dr. Mare Altosaar, Dr. Tiit Varema, Dr. Jaan Raudoja, Reelika Kaupmees, they also gave me lots of support in my experimental work. Then, I'd like to thank other stuff who help me during my work in the lab, they are Dr. Valdek Mikli, Dr. Taavi Raadik, Dr. Arvo Mere, and Dr. Mati Danilson. Last, I want to thank my family, due to their support, let me to finish my master degree and I would like to thank lots of friends both from my home country and here, in Estonia, they gave me a lot of spiritual help.

In this thesis, $\text{Cu}_2\text{CdGeSe}_4$ powder materials were synthesized from binary compounds (CuSe, CdSe) and elemental metal powders (Ge) and Se at temperatures - 500, 600, and 700 °C in the liquid phase of KI and CdI_2 as flux materials in evacuated quartz ampoules. Phase analysis by Raman spectroscopy and X-ray diffraction showed that $\text{Cu}_2\text{CdGeSe}_4$ powder synthesized at 500 °C had a tetragonal structure and powders synthesized at temperatures 60 °C and 700 °C had orthorhombic structure. The band gap obtained from external quantum efficiency measurements was found to be 1.27 eV for orthorhombic structured powders and 1.14 eV for tetragonal structured powders. The best solar cell fabricated from the $\text{Cu}_2\text{CdGeSe}_4$ powder showed the conversion efficiency of 4.21 % (active area), with an open-circuit voltage of 0.46 V, a short-circuit current density of 23.3 mA/cm² and fill factor of 39 %. The Raman and energy dispersive X-ray spectroscopy (EDX) results indicated that the phase and elemental composition of the product material change by changing the growth temperature and chemical etching. According to the EDX, scanning electron spectroscopy and Raman analysis the chemical input formula of $\text{Cu}_2\text{CdGeSe}_4$, results in the co-existence of CdSe secondary phase in the experimental synthesis conditions. The sieving analysis revealed that median particle size of produced powder crystals increased with increasing synthesis temperature and duration.

Key Words: $\text{Cu}_2\text{CdGeSe}_4$, monograin powders, flux materials, master thesis

List of abbreviations and symbols

CdI₂ - Cadmium iodide

CZTSSe - copper zinc tin sulfide/ selenide

CCGSe - Cu₂CdGeSe₄

CIGS - Cu(In,Ga)Se₂

EC - Conduction band

EG - Band gap

EF - Fermi level

EV - Valence band

EDX - Energy-dispersive X-ray spectroscopy

HT- high-temperature

KI - Potassium iodide

KCN - Potassium cyanide

KOH - Potassium hydroxide

LT- low-temperature

MGL - Monograin layer solar cell

PV - Photovoltaic

PCE - power conversion efficiency

QE - quantum efficiency

SEM - Scanning electron microscopy

XRD - X-ray diffraction

INTRODUCTION

As we all know, energy demand in the world increases with the development of science and technology. Nowadays majority of energy produced by fossil fuels, not only it has some bad impacts to our environments but also fossil energy is limited on the earth. Therefore, developing sustainable energy has become necessary and indispensable. Currently, photovoltaics, which directly convert solar energy into electricity, offer a practical and sustainable solution to the challenge of meeting the increasing global energy demand. The implementation of solar energy is a fast growing sector due to its abundant and inexhaustible energy resource, less greenhouse gases emission and an effective renewable alternative to conventional fossil fuels.

Nowadays, solar cells are not only recognized as an alternative to conventional fossil fuels for providing power, but also they are decreasing the impact of environmental damage caused by conventional fossil fuels. There are developed many different technologies for solar cells production, such as single crystal silicon, multi-crystalline silicon and thin film solar cell. Thin film solar cells can be made from a variety of materials, including amorphous silicon (which has no crystalline structure), gallium arsenide (GaAs), copper indium diselenide, cadmium telluride (CdTe) [1], copper indium gallium diselenide (Cu(In,Ga)Se_2) [2] and copper zinc tin sulfide/selenide (CZTSSe) [3].

The large group of quaternary and ternary copper chalcogenides has attracted considerable attention due to their suitable properties for thin film solar cell absorbers. Among them the $\text{Cu}_2\text{CdGeSe}_4$ (CCGSe) compound is maybe less studied, therefore, it motivates researcher to do research on the quaternary $\text{Cu}_2\text{CdGeSe}_4$ due to its suitable physical and electronic properties [4]. Its phase stability and electronic structure have been studied with ab initio calculations [5]. In this thesis, the synthesis of $\text{Cu}_2\text{CdGeSe}_4$ monograin powders in the liquid phase of KI and CdI_2 at different temperatures (500, 600 and 700 °C) were studied.

The objectives of this work were to study the growth of $\text{Cu}_2\text{CdGeSe}_4$ monograin powders in molten flux materials- KI and CdI_2 , and to characterize the morphology, compositional, structural and electrical properties of $\text{Cu}_2\text{CdGeSe}_4$ powders with the aim to use these powders as absorber materials in monograin layer solar cells. The thesis is based on the experimental work carried out in the Laboratory of Photovoltaic Materials at the Department of Materials and Environmental Technology, in the Tallinn University of Technology.

1. LITERATURE REVIEW AND THE OBJECTIVE OF STUDY

1.1 Principles of solar cell

Solar cells or photovoltaic cells are electronic devices that convert the energy of light directly into electricity by using semiconducting materials, which have photovoltaic (PV) effect. The photovoltaic effect is a physical and chemical phenomenon, which creates voltage and electric current in a material upon exposure to light. It was first observed by Alexandre-Edmond Becquerel in 1839 [6-7]. The PV effect was first studied in solids, such as selenium, in the 1870s. In the 1880s, there was only 1 - 2 % efficiency for selenium photovoltaic cells in converting light to electricity [8]. In the 1920s and 1930s, quantum mechanics laid the theoretical foundation for our present understanding of PV [9]. Solar cells are made of semiconductors, which are crystalline solid materials with resistivity values between those of conductors and insulators [10].

Nowadays, solar cells technologies have experienced three generations development until now in order to get high-efficiency and low-cost solar cell. Polycrystalline silicon is used in an attempt to cut manufacturing costs, although the resulting cells are not as efficient as single crystal silicon in the first generation solar cell technology [11]. Second generation solar cell technology is thin film solar cells. Although they tend to sacrifice some efficiency, thin film solar cells are simpler and cheaper to produce. For the third generation of high-efficiency thin-film technology, where efficiency can be increased merely by adding more cells of different bandgap to a cell stack, at the expense of increased complexity and spectral sensitivity [12].

A diode composed by a p-type semiconductor and an n-type semiconductor is called as a solar cell. The majority carriers in p-type semiconductor are holes and free electrons are minority carriers, while the free electrons are majority carriers in n-type semiconductor and holes are minority carriers. When the n-type semiconductor meets the p-type semiconductor, the majority carriers of p-type and n-type will diffuse each other, which means the majority carrier-holes in p-type material will diffuse to n-type material and the majority carrier-free electron in n-type material diffuse to p-type material. This diffusion creates an electron-hole free region in a very short distance at the interface region. This thin layer is called depletion region. The electric field will be build-up with the diffusion of p- and n-type materials, moreover, the diffusion will be stopped until the electric field is enough high to resist diffusion (see Figure 1.1). The electric field created would drift the minority carrier in the opposite direction across the junction. When the drift carrier and diffused carrier are balanced in terms of magnitude and in opposite direction, which mean attain the equilibrium [13].

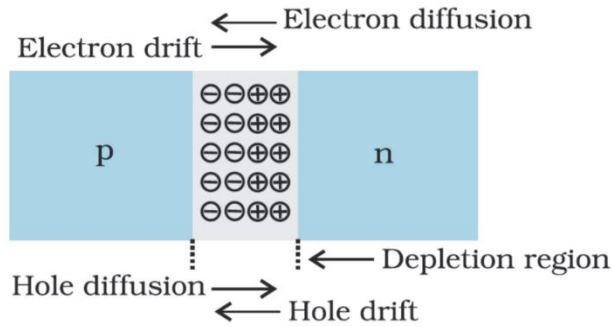


Figure 1.1 Scheme of the formation of p-n junction [14].

When the solar cell is exposed to light, the solar cell produces both a current and a voltage to generate electric power. Due to the influence of built-in electric field, electrons can drift to n-region and holes can easily drift to p-region, so this drift current generates the electric current. If the p-n junction is connected to external load with metal wires, it will produce the electric current in the external circuit to complete whole process of conversion of light into electricity (Figure 1.2) [15].

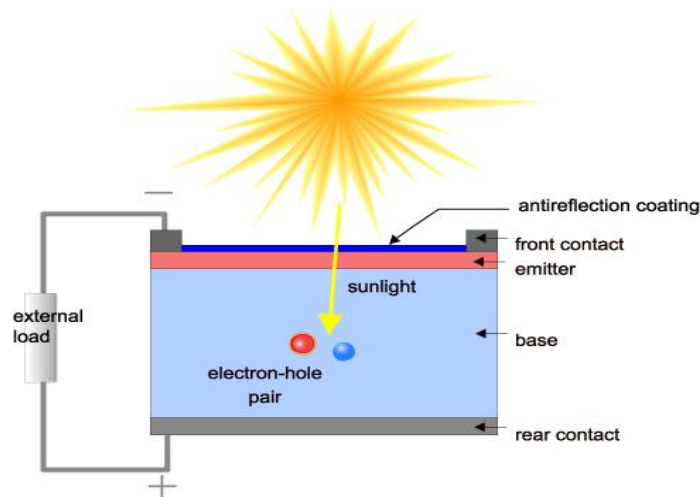


Figure 1.2 Scheme of photovoltaics generate electricity [15].

1.1.1 Review of solar cell absorber materials

In the past decades, a tremendous amount of research work has been carried out in the relevant fields and many types of solar cells materials have been developed and tested due to technological improvement, cost reductions in materials and government support for renewable energy based electricity production [16]. However, there are still a long way for satisfying the various requirements demanded, and many critical issues remain or are being studied, such as band gap (1.1 - 1.5 eV), high optical absorption ($\alpha > 10^4 \text{ cm}^{-1}$), a low recombination velocity and

should be able to form a good electronic junction. The final aim of most of the issues being studied is to improve the conversion efficiency of solar cells [17].

There have already been attempted many types of photovoltaics materials, such as semiconductor materials, organic dyes, conducting polymers, as well as their combinations. Currently, the efficiency of some primary materials for solar cell encompasses silicon (26.7 %) [18], gallium arsenide (28.8 %) [19], indium phosphide (24.2 %) [20], gallium indium phosphide (21.4 %) [21], Cu(In,Ga)Se_2 (22.6 %) [22], CdTe (22.1 %) [23] and $\text{Cu}_2\text{ZnSn(S,Se)}_4$ (12.6 %) [24]. Figure 1.3 below shows a scheme of classification of solar cells based on primary active material.

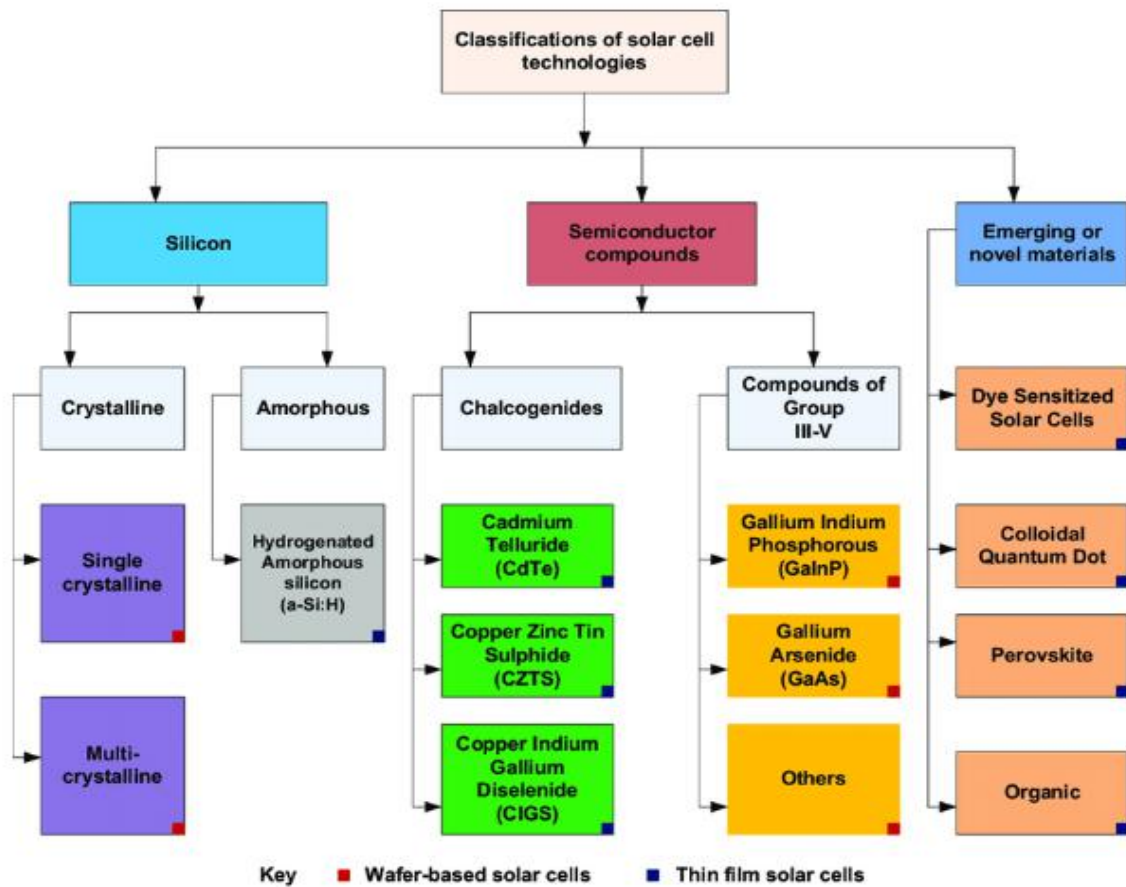


Figure 1.3 Classification of solar cells based on the primary active material [25].

Today, silicon is recognized as the most important semiconductor material for photovoltaic application. Currently, the solar cells based on silicon dominate the PV market, as they have demonstrated high power conversion efficiencies, up to 27 % [26]. Silicon materials are mainly divided into monocrystalline, polycrystalline (or multicrystalline) and amorphous by their crystal structure. Currently, the method of using wafer-based crystalline silicon have been studied to produce solar cells due to stable photo-conversion efficiency and it can be processed into efficient, non-toxic and very reliable PV cells [27]. Meanwhile, crystalline silicon cells still have some drawbacks, e.g., high level requirements for material purification, the module form factor

restrictions, batch-based cell production and poor absorber of light due to its indirect energy band gap of roughly 1.1 eV at room temperature, etc [28, 29]. Due to high power conversion efficiency, the attractive device stability as well as a much larger absorption coefficient across the solar radiation spectrum, amorphous silicon solar cell have been of long-standing interest as a thin-film, low-cost alternative to bulk crystalline silicon cells [30]. However, although as a second-generation thin-film solar cell technology, amorphous silicon was once expected to become a major contributor in the fast-growing worldwide photovoltaic market, it has since lost significance due to strong competition from conventional crystalline silicon cells and other thin-film technologies such as CdTe and Cu(In,Ga)Se₂.

Thin-film solar cells are the second generation solar cells that are made by depositing one or more thin layers of photovoltaic material on a substrate, such as glass, plastic or metal. Several technologies, including CdTe, GaAs and Cu(In,Ga)Se₂, have applied in thin-film solar cells. CdTe has been the leading thin-film PV technology based on global installed capacity. For this type of thin-film technology, efficiency has reached 22.1 % [23]. CuIn_xGa_{1-x}Se₂ (CIGS), the band gap of this type of material, which is high enough to cover the optimum region of band gaps for solar cells based on single-junction, but the best devices are fabricated at a band gap of 1.2 eV [28]. The record efficiency for laboratory-based CIGS devices is 22.6 % [22]. GaAs, which is a form of single junction III-V semiconductor that is well suited for photoelectric effects, it is perfectly appropriate to the solar spectrum due to high optical absorption coefficient, very low non-radiative energy loss, a near optimum direct band gap and good values of minority carrier lifetimes and mobility [31], the efficiency of GaAs-based solar cells of converting sunlight to electricity is 28.8 % and 24.1 % for lab cells and modules, respectively [32]. Although, a key disadvantage of this type material is the high cost in terms of producing epitaxial layers or device quality substrates as compared to crushing commercial edge associated with silicon [33].

In addition, CdTe and CIGS have a constituent element that are limited resource in the earth's crust, such as indium is extremely scarce [34], and more suitable band gap is also necessary to develop PV cells. The large group of quaternary and ternary copper chalcogenides has attracted considerable attention due to their suitable properties for thin film solar cell absorbers. The record efficiency of quaternary Cu₂ZnSn(S,Se)₄ (CZTSSe) based cells are still only 12.6 % [24]. This difference has also motivated research on other quaternary copper chalcogenides with suitable band gap energy for solar cell absorber. Among them the Cu₂CdGeSe₄ (CCGSe) compound is maybe less studied, but it has p-type conductivity and very promising properties with a band gap energy about 1.20 - 1.29 eV [35, 36].

1.2 Material properties of $\text{Cu}_2\text{CdGeSe}_4$

1.2.1 Crystal structure of $\text{Cu}_2\text{CdGeSe}_4$

$\text{Cu}_2\text{CdGeSe}_4$ has two crystal structure modifications such as the tetragonal structure with a $I-42m$ space group and an orthorhombic structure with a $Pmn21$ space group [37, 38]. The orthorhombic crystal structure is dominating at higher temperatures ($T > 605$ °C) while a tetragonal crystal structure is obtained at lower temperatures [39, 40]. It is reasonable to believe, that somewhat different reported E_g values are related to coexistence of different crystal structures.

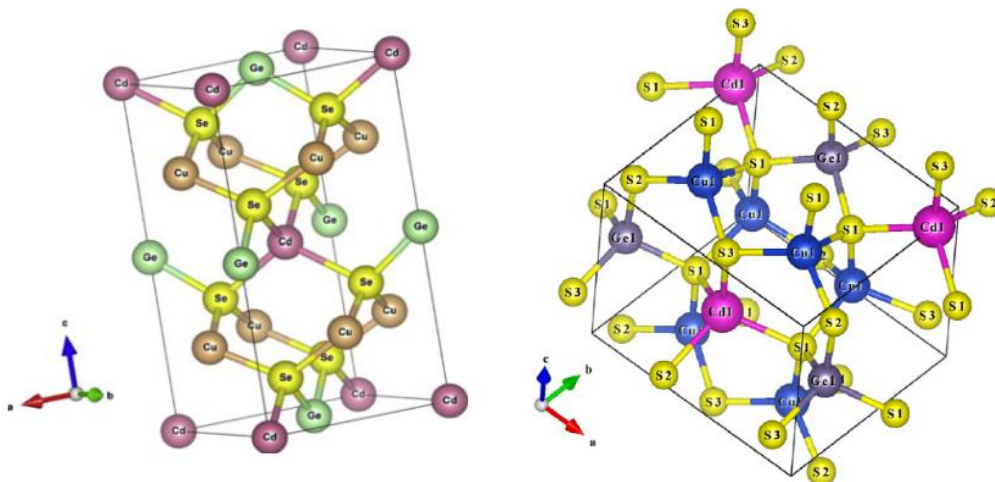


Figure 1.4 Tetragonal (left) LT- $\text{Cu}_2\text{CdGeSe}_4$ and HT- $\text{Cu}_2\text{CdGeSe}_4$ orthorhombic (right) structure [41, 42].

According to [36], the low-temperature (LT) modification of the $\text{Cu}_2\text{CdGeSe}_4$ were indexed assuming a tetragonal unit cell with the lattice parameters $a = 0.5748$ nm, $c = 1.1053$ nm. The high-temperature (HT) modification have lattice parameters $a = 0.8088$ nm, $b = 0.6875$ nm, $c = 0.6564$ nm [36].

The crystal structure of LT- $\text{Cu}_2\text{CdGeSe}_4$ and HT- $\text{Cu}_2\text{CdGeSe}_4$ is usually presented as the packing of selenium tetrahedra centered on germanium atoms. Copper and cadmium atoms are located in the voids between these tetrahedra (Figure 1.4).

In the tetragonal LT- $\text{Cu}_2\text{CdGeSe}_4$ the coordination polyhedra of all cations are tetrahedra formed by four Se atoms. Although all metal (Me) - Se bond lengths are equal for each cation, the tetrahedra are slightly distorted since the Se-Me-Se valency angles differ from the regular tetrahedral angle 109.5° . In the HT modification structure all atoms also have a tetrahedral surrounding but one crystallographic position is occupied by a statistical mixture ($M = 0.5 \text{ Cu} + 0.5 \text{ Cd}$). The coordination tetrahedra of cations and anions are distorted which

indicates some disordering of the HT-Cu₂CdGeSe₄ structure [38]. In addition, the Ge-Se bond lengths in tetragonal LT-Cu₂CdGeSe₄ are in good agreement with the sum of the ionic radii [$r(\text{Ge}^{4+}) = 0.053 \text{ nm}$ and $r(\text{Se}^{2-}) = 0.184 \text{ nm}$] while the Cu-Se and Cd-Se bond lengths are slightly shorter than the respective sum [$r(\text{Cu}^+) = 0.074 \text{ nm}$, $r(\text{Cd}^{2+}) = 0.092 \text{ nm}$] [38]. The interatomic distances in orthorhombic HT-Cu₂CdGeSe₄ are generally longer than those for the tetragonal modification, which leads to a slight increase of the volume cell at the same number of formula units per unit cell [38]. The density of the tetragonal and orthorhombic modifications are 5.712 g/cm³ and 5.638 g/cm³, respectively [42].

In addition, some peculiarities of the tetragonal \leftrightarrow orthorhombic structure transformation have been discussed. In the study [38] was supposed that there is a similarity with the sphalerite \leftrightarrow wurtzite transformation while taking into account that the tetragonal and orthorhombic modifications derive from the zinc blende and wurtzite structures, respectively. As the structure reconstruction demands a break of bonds, the transformations proceed slowly and metastable modifications can be persistent for a long time [38].

1.2.2 Synthesis methods of Cu₂CdGeSe₄

Cu₂CdGeSe₄ have been synthesized by different methods, such as the horizontal gradient freezing method [36], directional solidification method [35], a horizontal variation of Bridgman method [41], by solid-state reaction in sealed evacuated quartz ampoules [38, 39, 43] and chemical vapor transport reactions where iodine acts as transport agent [44].

In the study [38], the LT- and HT-Cu₂CdGeSe₄ compounds were synthesized in the evacuated quartz containers. The maximum temperature of the synthesis (900 °C) was chosen according to the melting temperature of Cu₂CdGeSe₄ ($T_{\text{melt}} = 840 \text{ °C}$ [45]). After isothermal annealing at that temperature for 2 hours, the HT-Cu₂CdGeSe₄ was obtained by cooling the material to 400 °C with a rate of 15 °C/h and quenched in cold water. In order to produce LT-Cu₂CdGeSe₄, the material was slowly cooled to 400 °C and annealed at this temperature for 250 hours, which followed by slow cooling to room temperature (RT).

According to [36], the bulk crystals of HT-Cu₂CdGeSe₄ were grown using the horizontal gradient freezing method from the respective melts. The starting materials were sealed in a quartz tube under vacuum of $\sim 10^6$ Torr. The quartz tube was first heated to 950 - 975 °C for 20 h, and held at this temperature for 24 h. Then, the whole zone was cooled electrically at a speed of 6 - 10 °C/h, keeping the temperature gradient of 3 °C/cm. From the optical absorption measurements, the

band gap of synthesized $\text{Cu}_2\text{CdGeSe}_4$ compound was 1.2 eV. Single crystals of the LT- $\text{Cu}_2\text{CdGeSe}_4$ obtained using directional solidification had optical energy gap value 1.29 eV [35].

In conclusion, there have been used several different methods for synthesis of the $\text{Cu}_2\text{CdGeSe}_4$ compound. Two polymorphous modifications were reported in several studies: an orthorhombic high-temperature modification and a tetragonal low-temperature modification. The HT- $\text{Cu}_2\text{CdGeSe}_4$ modification was generally obtained by annealing the samples at temperature over 400 °C followed by quenching the samples into water and LT- $\text{Cu}_2\text{CdGeSe}_4$ modification was produced by annealing at high temperatures ($T_{\text{ann}} > 400$ °C) followed by very slow cooling to RT. In this thesis, the task was synthesis $\text{Cu}_2\text{CdGeSe}_4$ monograin powders with both modifications.

1.2.3 The phase relations in the $\text{Cu}_2\text{Se-CdSe-GeSe}_2$ system

In the quasi-ternary $\text{Cu}_2\text{Se-CdSe-GeSe}_2$ system [45], it shows binary and ternary compounds which reveal semiconductor properties and have wide practical application. Moreover, the $\text{Cu}_2\text{CdGeSe}_4$ were formed in this system. However, it might become a challenge to produce homogeneous single phase $\text{Cu}_2\text{CdGeSe}_4$ absorber material due to the existence of number of elements and secondary phases.

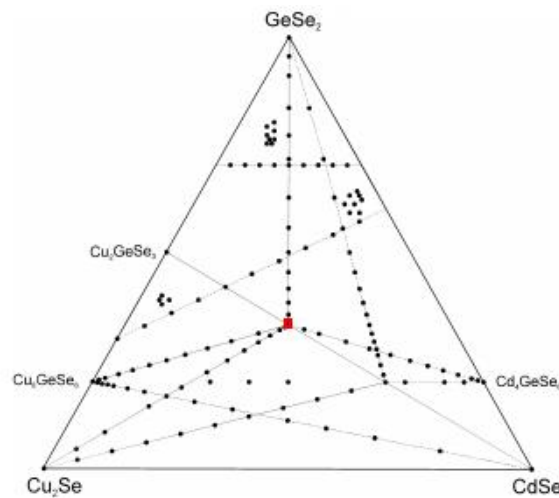


Figure 1.5 The quasi-ternary system $\text{Cu}_2\text{Se-CdSe-GeSe}_2$ [45].

In the Figure 1.5 is presented $\text{Cu}_2\text{Se-CdSe-GeSe}_2$ ternary phase diagram. All dots are presenting different alloys, which were prepared in [45] to study this system. For this thesis, the $\text{Cu}_2\text{Se-CdSe}$, $\text{Cu}_2\text{Se-GeSe}_2$, CdSe-GeSe_2 and $\text{Cu}_2\text{GeSe}_3\text{-CdSe}$ sections were taken into consideration. The existence region of $\text{Cu}_2\text{CdGeSe}_4$ is indicated by a small red square in the center [45].

In this thesis, the $\text{Cu}_2\text{CdGeSe}_4$ was synthesized by monograin powder technology. The metal-chalcogenide binaries such as CuSe and CdSe , elemental Ge and Se were used as precursor

materials. Therefore, the formation of different compounds in the following systems has to be considered.

1.2.3.1 Cu₂Se-CdSe quasi-binary system

According to [46], the diagram of the Cu₂Se-CdSe system belongs to the simple eutectic type with limited solubility of the components in the solid state (Fig. 1.6). The eutectic point corresponds to the composition 53 mol% CdSe and temperature 910 °C. Solid solutions based on Cu_{1.9}Se exist within the limits 0 - 50 mol% CdSe. With decreasing temperature, the solubility clearly decreases and at 602 °C it is 8 mol% CdSe. The solubility on the side of CdSe is 3.5 mol% Cu_{1.9}Se at the eutectic temperature and decreases to 0.4 mol% Cu_{1.9}Se when the temperature decreases to 600 °C.

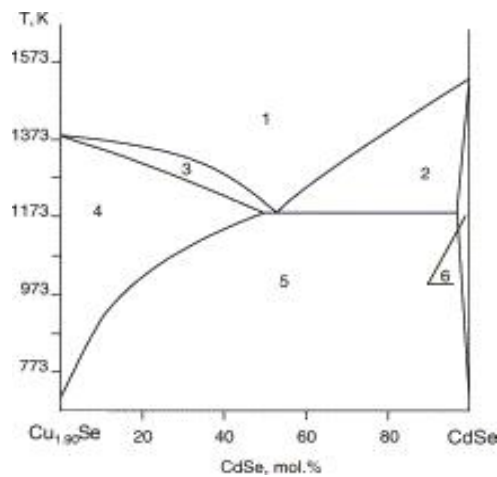


Figure 1.6 Phase diagram of the Cu₂Se–CdSe system: (1) L, (2) L + CdSe, (3) L + Cu_{1.9}Se, (4) Cu_{1.9}Se, (5) Cu_{1.9}Se + CdSe, (6) CdSe.

1.2.3.2 The Cu₂Se-GeSe₂ system

The Cu₂Se-GeSe₂ system has been investigated several times. The first investigation was carried out by Garcaly *et al* [47]. Due to some contradictions regarding the determination of melting type of Cu₂GeSe₃ and the occurrence of Cu₈GeSe₆, the system was re-investigated by Piskach *et al*. [43]. It was confirmed, that two ternary compounds Cu₂GeSe₃ and Cu₈GeSe₆ reveal in the system Cu₂Se-GeSe₂ (Fig. 1.7). The ternary Cu₂GeSe₃ compound melts congruently at 780 °C. The peritectic reaction $L + \text{Cu}_2\text{Se} \rightleftharpoons \text{Cu}_8\text{GeSe}_6$, taking place at 810 °C [43], corresponds to the formation of Cu₈GeSe₆. Two polymorphous transformations were established for Cu₈GeSe₆ phase at 710 °C and 60 °C. Cu₂GeSe₃ crystallizes in an orthorhombic symmetry (space group *Imm2*), and two modifications of Cu₈GeSe₆ are hexagonal [45].

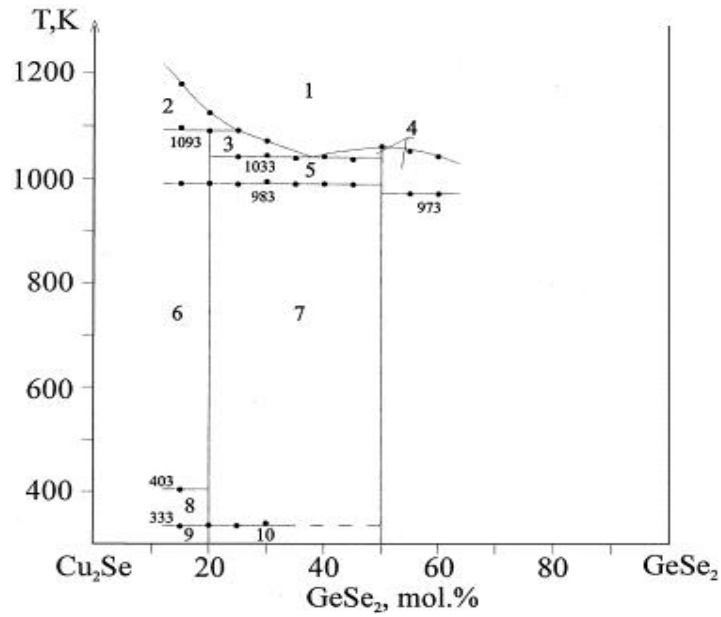


Fig. 1.7 Phase diagram of the Cu_2Se – GeSe_2 system in the region 15 – 60 mol% GeSe_2 : (1) L, (2) L + α - Cu_2Se , (3) L + α - Cu_8GeSe_6 , (4) L + Cu_2GeSe_3 , (5) Cu_2GeSe_3 + α - Cu_8GeSe_6 , (6) β - Cu_8GeSe_6 + α - Cu_2Se , (7) Cu_2GeSe_3 + β - Cu_8GeSe_6 , (8) β - Cu_8GeSe_6 + β - Cu_2Se , (9) γ - Cu_8GeSe_6 + α - Cu_2Se , (10) Cu_2GeSe_3 + γ - Cu_8GeSe_6 .

1.2.3.3 The CdSe - GeSe_2 system

According to [45], in the CdSe - GeSe_2 system was found the Cd_4GeSe_6 compound, which melts incongruently at 863 °C. An eutectic forms between GeSe_2 and Cd_4GeSe_6 , melting of the eutectic takes place at 716 °C. The composition of the eutectic point is 30 mol% CdSe . At 547 °C, GeSe_2 dissolves 2.1 mol% CdSe and CdSe dissolves 0.7 mol% GeSe_2 .

1.2.3.4 The Cu_2GeSe_3 - CdSe system

Figure 1.8 presents the phase diagram of the Cu_2GeSe_3 - CdSe [45]. It is confirmed that $\text{Cu}_2\text{CdGeSe}_4$ exists in this system, which melts incongruently at 840 °C and forms eutectic with Cu_2GeSe_3 [45]. The regions for different phases are bordered with lines. The three yellow horizontal lines represent the temperatures at 500 °C, 600 °C and 700 °C, which are used for the monograin powder synthesis in this thesis. The sign ϵ is another quaternary phase with composition $\text{Cu}_2\text{Cd}_3\text{GeSe}_6$, which is formed by a peritectic process $\text{L} + \text{CdSe} \rightleftharpoons \text{Cu}_2\text{Cd}_3\text{GeSe}_6$ at 900 °C and decomposes $\text{Cu}_2\text{Cd}_3\text{GeSe}_6 \rightleftharpoons \text{Cu}_2\text{CdGeSe}_4 + \text{CdSe}$ at 736 °C by the eutectoid reaction [45].

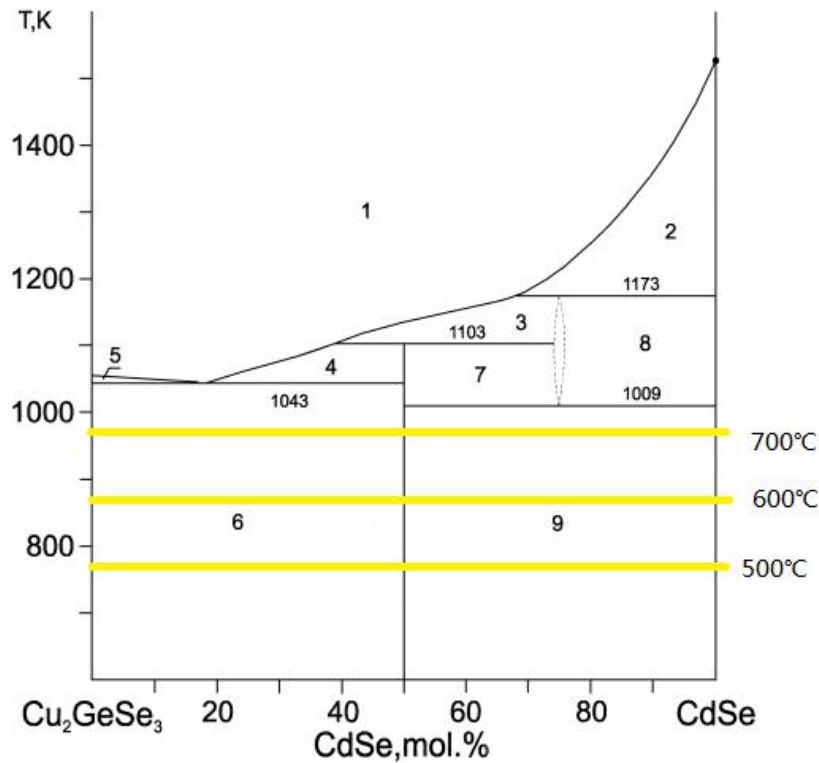


Figure 1.8 Phase diagram of the quasi-binary section $\text{Cu}_2\text{GeSe}_3\text{-CdSe}$: (1) L, (2) L + CdSe, (3) L + ϵ , (4) L + $\text{Cu}_2\text{CdGeSe}_4$, (5) L + Cu_2GeSe_3 , (6) $\text{Cu}_2\text{GeSe}_3 + \text{Cu}_2\text{CdGeSe}_4$, (7) $\epsilon + \text{Cu}_2\text{CdGeSe}_4$, (8) $\epsilon + \text{CdSe}$, (9) $\text{Cu}_2\text{CdGeSe}_4 + \text{CdSe}$.

1.2.4 Optical and electrical properties of $\text{Cu}_2\text{CdGeSe}_4$

As we all know, the optical absorption coefficient is one of the most crucial evaluation criterions in application of the photoelectric materials. Recently, the quaternary compounds $\text{I}_2\text{-II-IV-VI}_4$ (I = Cu, Ag; II = Zn, Cd, Hg; IV = Si, Ge, Sn; VI = S, Se) have drawn wide interest for their potential applications in thin-film solar cells due to their p-type conductivity and high optical absorption ($> 1 \times 10^4 \text{ cm}^{-1}$) [48].

Among these quaternary alloys $\text{Cu}_2\text{CdGeSe}_4$ has strong optical anisotropy and the energy gap value is about 1.20 - 1.29 eV [35, 36]. Its phase stability and electronic structure have been studied with ab initio calculations [5]. Besides, two polymorphous modifications were reported in Ref. [38]: an orthorhombic high-temperature modification with the wurtzite-stannite structure and a tetragonal low-temperature modification with the stannite structure. And with the calculations of the total energy the ST structure of $\text{Cu}_2\text{CdGeSe}_4$ is more stable than the others, hence this phase is the ground-state structure [48].

1.3 Monograin powder technology

1.3.1 Overview of monograin technology

The thin-film technologies are the principal technologies used today for manufacturing solar cells [49]. The monograin layer technology (MGL) has a lot of advantages to overcome these shortcomings, such as the low cost, simple technology of materials and layers preparation and possibility of making devices of practically unlimited area. A main technological advantage is the separation between absorber and cell formations. In a word, the MGL combines the superior photoelectrical parameters of single crystals with the advantages of polycrystalline materials.

1.3.2 Monograin powder growth

Monograin powders are semiconductor materials with single-crystalline grain structure and narrow-disperse granularity, which are formed by the isothermal heating of precursor materials in the presence of liquid phase of a suitable solvent flux salt [50]. Single crystals can be obtained at temperatures higher than the melting point of the used flux salts and at temperatures lower than the melting point of the semiconductor itself [51]. Designing these single-crystalline grains instead of one traditional big one, which compile the advantages of monocrystalline and polycrystalline constructions, such as single-crystalline structures of every grain, uniform distribution of doping impurities and narrow granulometric composition [52]. In the powder growth process, it is very important for the characteristics of formed monograin powder crystals and the equilibrium conditions to control the synthesis temperature and amount of the flux salts [51].

From the constituent elements, from binary chalcogenides, from elemental metal alloys and chalcogen, all of these different precursors can form the stable quaternary compounds [53]. The precursors are divided different steps to react with each other during the material's formation-nucleation stage, either they can dissolve completely in the molten salt, with the nuclei of the formation of nuclei of the solid product in the liquid phase (growth of single crystals); or then initial solid particles of low-solubility precursors react with each other in the molten salt media, and the formed solid particles of the product compound start to recrystallize and grow resulting in monograin powder growth [54]. The volume of the used molten salt has to exceed the volume of voids between precursor particles, which can repel both the solid precursor particles and the formed powder particles from each other and to avoid sintering caused by the contracting capillary forces arising in the solid-liquid phase boundaries [51]. Synthesis in molten salts

enhances the rate of solid-state reactions due to the much higher diffusion rates between reaction components in the molten media [55], lower the reaction temperature, increasing the homogeneity of the solid product, and controlling the particle shape and size as well as their agglomeration rate.

1.3.2.1 Flux materials

Molten salts have proven to be useful to enhance the reaction rate as alternative reaction media and it allows fast diffusion of constituent elements through liquid phase. The synthesis of multicomponent compounds in the liquid phase of a flux provides uniform composition of produced materials [56]. The suitable flux material need to have low melting point, low vapor pressure and high solubility in water as well as an easy separation of the powder particles from the fluxes [17]. Several flux materials, such as NaI, KI, CdI₂, have been used for synthesis the quaternary compounds as absorber materials for solar cells. In this thesis, KI and CdI₂ as flux materials were used.

Potassium iodide has a rather higher melting temperature (681 °C) comparing with cadmium iodide (387 °C) and due to this doping of the synthesized absorber material with potassium and iodine could be presumable [17]. Although KI is rather stable in dry air, it can accelerate the decomposition when exposing to light and moisture. The aged and impure KI will be yellow due to the instability of KI in air, which is caused the slow oxidation of the salt to potassium carbonate and elemental iodine.

The CdI₂ structure consists of different stackings of CdI₂ sandwiches in each of which a layer of cadmium ions is sandwiched between two close packed layers of iodine ions. Cadmium iodide has a hexagonal shape, which is considered to be consisting of two layers of hexagonal closed pack iodine ion nested between them [57, 58]. Although the solubility will be higher with the increasing the temperature, the solubility of CdI₂ in water at 100 °C is 1250 g/L; while the solubility of KI is 2060 g/L at the same temperature.

1.3.3 Monograin layer solar cell

The monograin layer consists of a one crystal thick layer of grains of monograin powder embedded in an organic resin (epoxy). The material studied in the present work is used as p-type absorber material in the monograin layer solar cells. Both- the absorber quality and interface between the absorber and buffer layer are important issues for designing an efficient solar cell [57]. In Fig. 1.9 is presented the structure of typical MGL solar cell: graphite back contact/absorber crystal/CdS buffer/i-ZnO/ZnO: Al window layer/glass substrate. CdS buffer layer

is usually made by chemical bath deposition, *i*-ZnO and conductive ZnO: Al layers are deposited by RF sputtering. The formed structure is glued onto a glass substrate. Conductive graphite paste is used to make back contacts and Ag is used to make front collector to contact all layers.

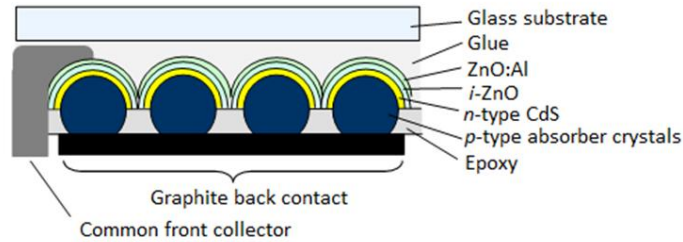


Figure 1.9 The device structure of MGL solar cell: graphite back contact/ absorber crystal/CdS buffer/*i*-ZnO/ZnO:Al window layer/glass substrate [59].

MGL solar cell has many advantages of polycrystalline materials and technologies and the high photoelectrical parameters of mono-crystalline: (1) low cost and simple technology of materials and devices; (2) the possibility of making flexible devices; (3) the possibility of using materials up to 100 % [58]. MGL technology allows the separation of materials formation from module fabrication. However, it still has some disadvantages, such as not all of the membrane area is working actively, because of epoxy between the powder crystals, some designs need powder grains of nearly equal size and perfect mono-crystalline structure, in addition, there are some problems of surface preparation of the grains in the MGL, which include chemical etching and thermal annealing treatment to clean the surface of crystals [58].

1.4 Summary of literature overview and the objective of the study

Currently, the solar cells, which directly convert solar energy into electricity, offer a practical and sustainable solution to the challenge of meeting the increasing global energy demand due to its abundant and inexhaustible energy resource, less greenhouse gases emission and an effective renewable alternative to conventional fossil fuels. Although silicon has dominated in the PV market, thin-film technologies have been a fast growing with reasonable conversion efficiency and cheaper materials compared to the silicon materials. Quaternary compounds $\text{Cu}_2\text{-II-IV-Se}_4$ (II-Zn, Cd, Hg; IV-Si, Ge, Sn) as absorber material have a wide interest for developing a new PV technology. Among them is also $\text{Cu}_2\text{CdGeSe}_4$ material, which has high absorption coefficient ($> 10^4 \text{ cm}^{-1}$) and suitable optical band gap (1.2 - 1.29 eV).

Monograin layer technologies combine the advantages of single crystals and polycrystalline materials, which are low cost and simple technology of materials and devices, and the possibility of making flexible devices and using the materials up to 100 %. The $\text{Cu}_2\text{CdGeSe}_4$ can be synthesized from different methods. Two polymorphous modifications were reported: an orthorhombic high-temperature modification with the wurtzite–stannite structure and a tetragonal low-temperature modification with the stannite structure. In this thesis, the metal-chalcogenide binaries such as CuSe and CdSe, elemental Ge and Se were used as precursor materials to synthesize $\text{Cu}_2\text{CdGeSe}_4$ monograin powders.

The existence of single phase $\text{Cu}_2\text{CdGeSe}_4$ is a narrow area of compositions in the equilibrium phase diagram, due to that, the choice of appropriate ratio of precursor materials, suitable flux materials, the synthesis time and temperature is very important. These technological parameters influence also the size and morphology of produced powder crystals. Monograin layer membrane consists of narrow fraction of crystals embedded into the polymer layer. Therefore, the fine adjustment of the crystal size and shape is one of the important factors for producing monograin powders for solar cells.

The overall aim of this research work was to study preparation conditions for the synthesis of $\text{Cu}_2\text{CdGeSe}_4$ monograin powders in the liquid phase of molten salts. Two flux materials - KI and CdI_2 were used in this thesis. The morphology and crystal size distribution, phase and elemental composition of powder crystals were studied by varying the synthesis temperature, time and the nature of flux material. Powders with suitable properties for PV applications were used in monograin layer solar cells as absorber materials and device characteristics were studied.

2. EXPERIMENTAL

In this study $\text{Cu}_2\text{CdGeSe}_4$ powder materials were synthesized from high-purity compounds (commercially available CdSe and self-synthesised $\text{CuSe}_{0.9587}$, $\text{CuSe}_{0.9936}$, $\text{CuSe}_{0.9889}$), elemental metal powder (Ge) and Se in the liquid phase of a flux material in evacuated quartz ampoules. Two different fluxes – cadmium iodide (CdI_2) and potassium iodide (KI) - were used. A major technological advantage of the usage of these salts as flux materials is the possibility of removing them after the growth process very easily by a simple dissolution process in distilled or DI water. The other advantage of fluxes is melting temperature lower than $\text{Cu}_2\text{CdGeSe}_4$ powder. The synthesis process of $\text{Cu}_2\text{CdGeSe}_4$ monograin powders in CdI_2 flux were performed at synthesis temperatures 500 °C, 600 °C and 700 °C for 120 hours and synthesis in KI flux was performed at 700 °C for 60 hours and 120 hours. Technological parameters of $\text{Cu}_2\text{CdGeSe}_4$ powder synthesis are summarized in Table 2.1.

Table 2.1: Synthesis parameters of $\text{Cu}_2\text{CdGeSe}_4$ powder materials

Material name	Synthesis flux	Synthesis temperature, °C	Synthesis time, h
Powder 1	CdI_2	500	120
Powder 2	CdI_2	600	120
Powder 3	CdI_2	700	120
Powder 4	KI	700	120
Powder 5	KI	700	60

2.1 Preparation of monograins

All $\text{Cu}_2\text{CdGeSe}_4$ powder materials were synthesized from binary compounds (CdSe and $\text{CuSe}_{0.9587}$, $\text{CuSe}_{0.9936}$, $\text{CuSe}_{0.9889}$), elemental metal powder (Ge) and selenium.

In the first experiment, binary compounds (CdSe , $\text{CuSe}_{0.9587}$, $\text{CuSe}_{0.9936}$, $\text{CuSe}_{0.9889}$), and elemental Ge powder were weighted in proportions needed for synthesis of four powders (Powder 1, 3, 4, 5) taking into account that final batch mass is approx. 15 g. The ratio of Cu:Cd:Ge was 2:1:1. The total mass of precursors was 52.092 g. The precursor mixture was ground in a ball mill. After grinding, the mass of the precursor's mixture was 51.376 g. Then the precursor mixture was poured into N_2 -filled quartz ampoule, the material was degassed under dynamic vacuum at 150 °C for 3.5 hours. Subsequently, the degassed precursor mixture was divided into four portions and proportional amount of Se was added to each batch. To prevent the evaporation of Se during degassing, it was added later. The final amounts of precursor mixtures for the $\text{Cu}_2\text{CdGeSe}_4$ synthesis were as follows: 17.019 g (powder 1), 13.832 g (powder 3), 14.179 g (powder 4), and 13.926 g (powder 5).

In the second experiment, powder 2 were mixed from the precursor materials (CuSe, CdSe, Ge, and Se) and grounded in an agate mortar. The following process was similar as used for preparing the previous powders. The amount of precursors for $\text{Cu}_2\text{CdGeSe}_4$ syntheses and the amount of flux were nearly equal to provide the volume of liquid phases enough for the monograin growth ($m_{\text{precursors}}/m_{\text{flux}} = 1:1$) (see Table 2.2). Before adding KI flux to the ampoule, this flux material was degassed in dynamic vacuum (continuous vacuum pumping) at temperatures up to 270 °C for dehydration; while it is not necessary to do the same treatment for CdI_2 as flux, it is more stable in air and without absorbing the water in air. After mixing the precursors and fluxes, the ampoules were sealed.

Table 2.2: Mass parameters of precursors and fluxes

Material	Mass of precursors, g	Mass of flux, g
Powder 1 (CdI_2)	17.019	17.0
Powder 2 (CdI_2)	14.953	14.9
Powder 3 (CdI_2)	13.832	13.8
Powder 4 (KI)	14.179	14.2
Powder 5 (KI)	13.926	13.9

After evacuation, the ampoules were sealed and placed to muffle furnace at room temperature. The time for heating up the furnace with the samples inside for required temperature was approximately 24 hours. Then the temperature was maintained at synthesis temperature 120 hours for materials (Powder 1, 2, 3, 4) and for material (Powder 5) it was 60 hours. The synthesis was terminated by taking samples out from the furnace and cooled to the room temperature in an air.

After opening the ampoules, the synthesized materials were separated from flux by leaching with distilled water. The washing process was carried out in an ultrasonic bath at 50 °C. Solid particles were separated by decantation until washing water became transparent. In case the synthesized powders were still visibly agglomerated after washing with water, the additional washing process with 10 % KCN +1 % KOH aqueous solution was performed for 30 minutes. Final washing was done with ultra-pure water until leaching solutions stayed transparent. The released monograin powders were dried in a hot-air thermostat.

2.1.1 Post-treatment of $\text{Cu}_2\text{CdGeSe}_4$ monograin powders

$\text{Cu}_2\text{CdGeSe}_4$ (Powder 4) was post-treated isothermally at elevated temperature before using them as absorber materials in monograin layer solar cells. The heat-treatment process was carried out in the chamber furnace at temperature of 500 °C for 1 hour. The post-treatment parameters were chosen according to paper [38]. Two samples from powder 4 were prepared in order to produce

HT-phase and LT-phase powders. The parameters of the samples for post-treatment experiments are listed in Table 2.3.

Table 2.3: The heat-treatment parameters of samples

Material	Fraction, μm	Mass of sample, g	Temperature, $^{\circ}\text{C}$	Time, h	Cooling regime
Powder 4/1	80-100	0.25	500	1	Quenched in water
Powder 4/2	80-100	0.25	500	1	Slow cooling with furnace

2.2 Characterization of monograins

2.2.1 Particle size determination method

There are different methods for determining the particle distribution. The choice of a particular method depends primarily on the dispersion status, i.e. on the degree of fineness of the sample. The oldest and best-known method is particle size determination by sieve analysis. The particle size distribution is defined via the mass. Sieve analysis is used to divide the particulate material into size fractions and then to determine the weight of these fractions. In this way a relatively broad particle size spectrum can be analyzed quickly and reliably.

The synthesized powder materials were sieved into narrow granulometric fractions between 38 to 500 μm . The sieves used separated the following fractions: 38-45, 45-56, 56-63, 63-75, 75-80, 80-90, 90-100, 100-112, 112-125, 125-140, 140-150, 150-160, 160-180, 180-200, 200-224, 224-250, 250- 500 μm . The sieving was performed on a vibrating machine (see Figure 2.1). The process was followed by manual sieving until the amount of the powder on the sieve stayed unchanged. The amount of material on one sieve was weighed with accuracy of 0.01g.



Figure 2.1 Scheme of sieving machine.

2.2.2 Raman spectroscopy

Raman spectroscopy is a spectroscopic technique used to observe vibrational, rotational and other low frequency modes in a system. When light interacts with matter, the photons, which make up the light, may be absorbed and scattered, or may not interact with the material and may pass straight through it. If the energy of an incident photon corresponds to the energy gap between the ground state of a molecule and an excited state, the photon may be absorbed and the molecule promoted to the higher energy excited state. The scattered photons can be observed by collecting light at an angle to the incident light beam. However, the main scattering technique used for molecular identification is Raman scattering [60]. Briefly, the laser light interacts with molecular vibrations in the sample, resulting in the energy of the laser photons being shifted up or down. The shift in energy is recorded and Raman spectrum is created.

In this study, the phase composition of the powders was studied by room-temperature micro-Raman spectroscopy using Horiba's LabRam HR 800 spectrometer equipped with a multichannel CCD detection system in the backscattering configuration using a 532 nm laser line with a spot size of 5 μm . The measurement error in Raman peak position is 0.5 cm^{-1} .

2.2.3 XRD analysis

The crystalline structure of monograin powders was characterized by X-ray diffraction (XRD) using a Rigaku Ultima IV diffractometer with monochromatic Cu K α radiation $\lambda = 1.54056 \text{ \AA}$ at 40 kV and 40 mA, using a D/teX Ultra silicon strip detector. For the identification of crystal phases, the Joint Committee on Powder Diffraction Standards (JCPDS) database was used. Lattice parameters were calculated using Rigaku PDXL Version 1.4.0.3 software. The XRD measurements of monograin powders were carried out by Dr. Arvo Mere at Tallinn University of Technology.

2.2.4 Scanning electron microscopy (SEM)

Scanning electron microscopy is one of most advanced methods providing analysis about the shape and surface morphology of the crystals. The SEM method enables to observe and characterize the materials on a nanometer-to-micrometer scale [61]. In SEM, the area of a sample is examined with a finely focused electron beam, which could be swept across the surface of the sample to form an image [61]. The specimen is bombarded by a convergent electron beam, which is scanned across the surface. This electron beam generates a number of different types of signals, which are emitted from the area of the specimen where the electron beam is impinging. The induced signals are detected and the intensity of one of the signals is amplified and used to as the

intensity of a pixel on the image on the computer screen. The electron beam then moves to next position on the sample and the detected intensity gives the intensity in the second pixel and so on [62]. The morphology of synthesized powder crystals was studied by high-resolution scanning electron microscope (HR-SEM) Zeiss ULTRA 55. The SEM images were made by Dr. Valdek Mikli at Tallinn University of Technology.

2.2.5 Energy dispersive X-ray spectroscopy (EDX)

Energy dispersive X-ray spectroscopy (EDX) is an analytical technique used for the chemical characterization or elemental analysis of a sample. EDX was used to determine the elemental composition of the synthesized monograin powders. The X-rays are detected by an energy dispersive detector, which displays the signal as a spectrum, or histogram of intensity versus X-ray energy. The energies of the characteristic X-rays allow the elements making up the sample to be identified, while the intensities of the characteristic X-ray peaks allow the concentrations of the elements to be quantified [63]. It is the same underlying principles for generation of X-rays and detection by EDX and SEM.

The bulk composition of the synthesized powder crystals were analyzed by EDX on Zeiss (HR-SEM) ULTRA 55 equipped with a backscattered detector and Bruker Esprit 1.8 system with an accelerating voltage of 20 kV. Compositional analyses were made from polished cross-section of individual crystals. The measurement error for elemental analysis is about 0.5 at%. The EDX measurements were carried out by Dr. Valdek Mikli at Tallinn University of Technology.

2.2.6 Grain resistance measurements

The hot-probe method is used for determining quickly whether a semiconductor sample is n-type or p-type. A multimeter, which has been adjusted to voltage mode, is attached to the sample, and a heat source, such as a soldering iron, is placed on one of the leads. The heat source will cause charge carriers (electrons in an n-type, holes in a p-type) to move away from the lead. The heat from the probe creates an increased number of higher energy carriers, which then diffuse away from the contact point. This will cause a voltage difference. For example, if a heat source is placed on the positive lead of a voltmeter connected to an n-type semiconductor, the voltage will increase with the heat increases. In contrast, if the heat source is connected to the positive line of the voltmeter of the p-type semiconductor, the voltage will be reduced. We can read the resistance of grains when turn the voltage mode to the resistance mode of the multimeter.

2.3 Solar cell characteristics

Completed solar cell structures were characterized by dark and light current-voltage (I-V) and external quantum efficiency measurements (EQE).

2.3.1 Current-Voltage measurements

Several parameters were used to characterize the efficiency of the solar cells. IV curves were measured to evaluate the main characteristics of solar cells, which are the open-circuit voltage (V_{oc}), short-circuit current density (J_{sc}), fill factor (FF) and efficiency (η).

In the figure 2.2, it shows the maximum delivered energy, $P_{max} = V_{max} \cdot I_{max}$; fill factor (FF), it shows the ratio of P_{max} to the product of $V_{oc} \cdot I_{sc}$, $FF = (V_{max} \cdot I_{max}) / (V_{oc} \cdot I_{sc})$; the power conversion efficiency of solar cell $\eta = V_{oc} \cdot I_{sc} \cdot FF / P_{in}$, where P_{in} is the power density of exiting illumination. Measurements were performed using Keithley 2400 source meter in dark and under standard test conditions light with illumination intensity of 100 mW/cm^2 (AM 1.5).

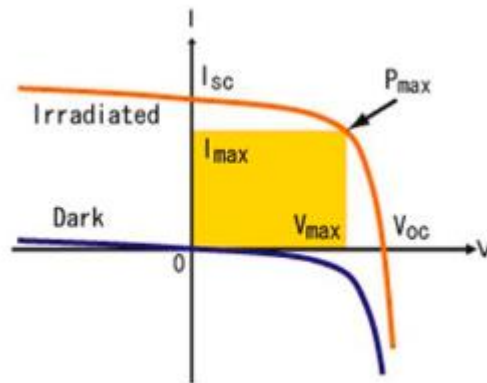


Figure 2.2 I-V characteristics of a solar cell at non-illuminated (dark) and illuminated conditions.

2.3.2 Quantum efficiency measurements

Unfortunately, the evaluation of E_g from the UV-VIS reflectance spectra of monograins is rather challenging. External quantum efficiency (EQE) analysis is an alternative method that can be used to estimate the effective band gap energy E_g^* of the synthesized absorber materials [64].

Spectral response measurements were performed in the spectral region of 350 - 1235 nm using a computer controlled SPM-2 prism monochromator. The generated photocurrent was detected at 0 V bias voltage at RT by using a 250 W halogen lamp. The EQE measurements were carried out by Dr. Mati Danilson at Tallinn University of Technology.

3. RESULTS AND DISCUSSIONS

3.1 Particle size distribution

Sieving analysis helps to estimate the particle size distribution of the monograins by evaluating their linear growth. The results of sieve analysis are generally expressed in terms of the percentage of the total weight of particles that passed through different sieves. The results of mechanical analysis are generally presented by semi-logarithmic plots known as particle-size distribution curves. The particle diameters are plotted in log scale, and the corresponding percent finer in arithmetic scale. The calculations are as follows:

$$\% \text{ retained on any sieve} = \frac{\text{weight of particles retained}}{\text{total weight of powder}} \times 100 \%$$

$$\% \text{ finer than an sieve size} = 100 \% - \Sigma \% \text{ retained}$$

Particle size fractions of $\text{Cu}_2\text{CdGeSe}_4$ lower than $38 \mu\text{m}$ and greater than $250 \mu\text{m}$ are left out while other fractions are taken as 100 %. Figure 3.1 shows the particle size distribution of monograin powders grown at different temperatures in CdI_2 molten salt and powders grown in KI flux for different times at 700°C . The black solid horizontal line marks 50 %, it shows the powder median grain size values (D_{50}) calculated from weight percent. The D_{50} is the size in microns that splits the distribution with half above and half below this diameter. The sieving analysis revealed that median particle size of produced powder crystals increased with increasing synthesis temperature and duration. Median sizes of particles are $25 \mu\text{m}$, $58 \mu\text{m}$ and $139 \mu\text{m}$ for powders synthesized in CdI_2 at 500 , 600 and 700°C , respectively. Median sizes of particles are $112 \mu\text{m}$ and $132 \mu\text{m}$ for powders synthesized in KI flux for 60 hours and 120 hours, respectively.

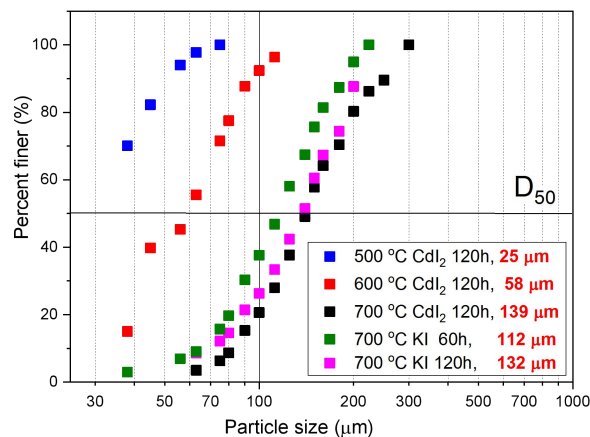


Figure 3.1 Particle size distribution obtained from sieving analysis for all powders.

3.2 Morphology of $\text{Cu}_2\text{CdGeSe}_4$ monograin powders

3.2.1 Shape analysis by optical microscopy

Figure 3.2 presents the optical microscope images of $\text{Cu}_2\text{CdGeSe}_4$ powder crystals grown in molten CdI_2 at different synthesis temperatures - 500 °C, 600 °C, and 700 °C, respectively. Fig. 3.2 (a) shows that powder crystal synthesized at 500 °C in CdI_2 flux had sharp crystal edges and crystal planes are not shiny. In the Fig. 3.2 (c), the crystals synthesized at 700 °C show more rounded grain edges and clean, shiny planes. Powder crystals, which were synthesized at 600 °C had bar-shaped particles with sharp edges and shiny planes Fig. 3.2 (b).

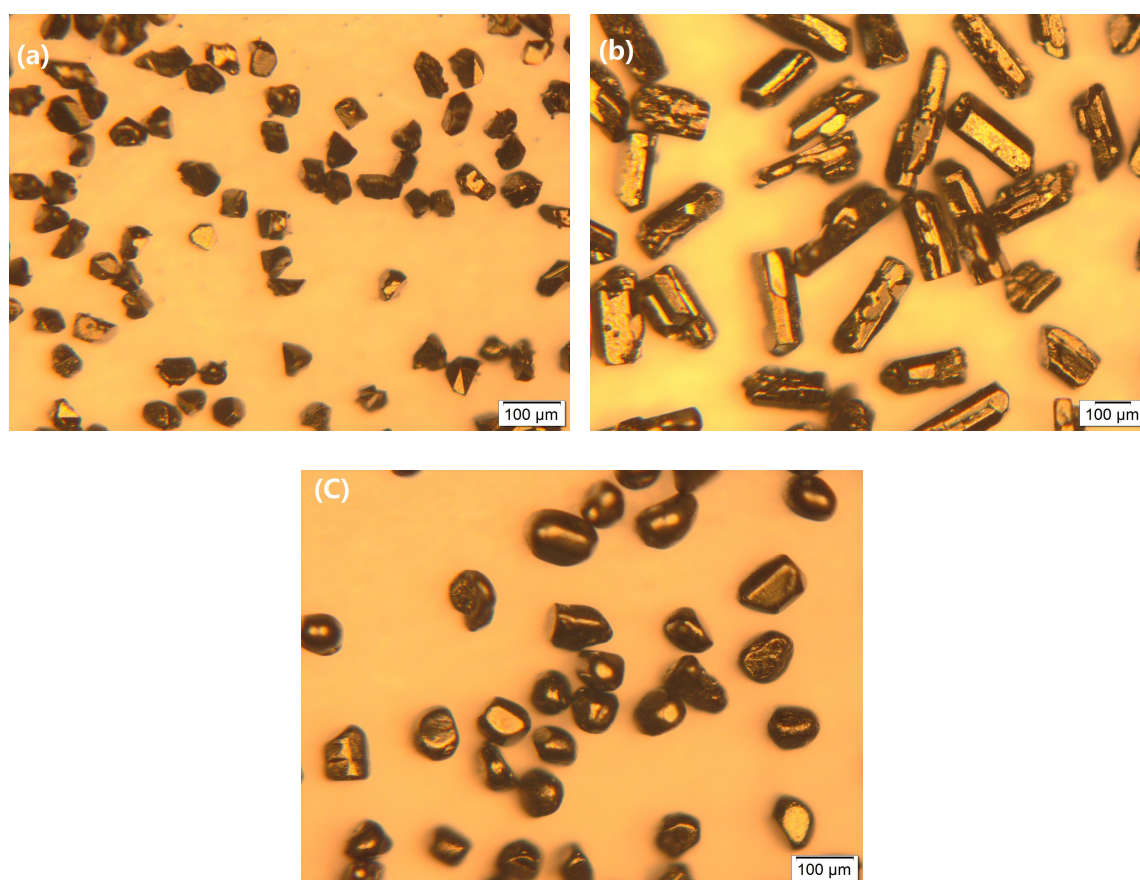


Figure 3.2 The optical microscope images of $\text{Cu}_2\text{CdGeSe}_4$ monograin powders (fraction 63-75 μm) synthesized in CdI_2 at temperatures a) 500 °C (Powder 1), b) 600 °C (Powder 2) and c) 700 °C (Powder 3).

Figure 3.3 shows the optical microscope images of $\text{Cu}_2\text{CdGeSe}_4$ powder crystals grown in two different fluxes - KI and CdI_2 at the same synthesis temperature 700 °C. The image 3.3 (a) shows more rounded grain edges in the CdI_2 , while the sharp edges of grains were revealed in the KI , shiny planes and there are still some bar-shaped particles simultaneously in the Figure 3.3 (b).

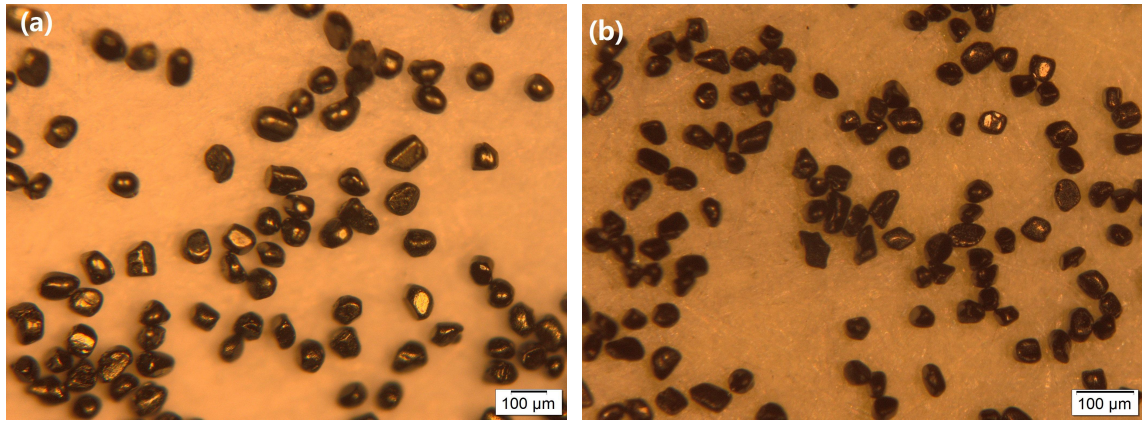


Figure 3.3 The optical microscope images of $\text{Cu}_2\text{CdGeSe}_4$ monograin powders (fraction 63-75 μm) synthesised at temperature 700 $^\circ\text{C}$ a) in CdI_2 flux (Powder 3) and b) in KI flux (Powder 4).

3.2.2 Morphology analysis by scanning electron microscopy (SEM)

Figures 3.4 (a) - (c) present the SEM images of $\text{Cu}_2\text{CdGeSe}_4$ powder crystals grown in molten CdI_2 at different synthesis temperatures - 500 $^\circ\text{C}$, 600 $^\circ\text{C}$ and 700 $^\circ\text{C}$, respectively. In addition to single crystalline monograins, also some sintered grains were detected. Figure 3.4 (c) shows the SEM image of $\text{Cu}_2\text{CdGeSe}_4$ powder crystals synthesised at 700 $^\circ\text{C}$ for 120 hours, the majority of as grown monograins have ball shape with very rounded edges and the plain surfaces are smooth.

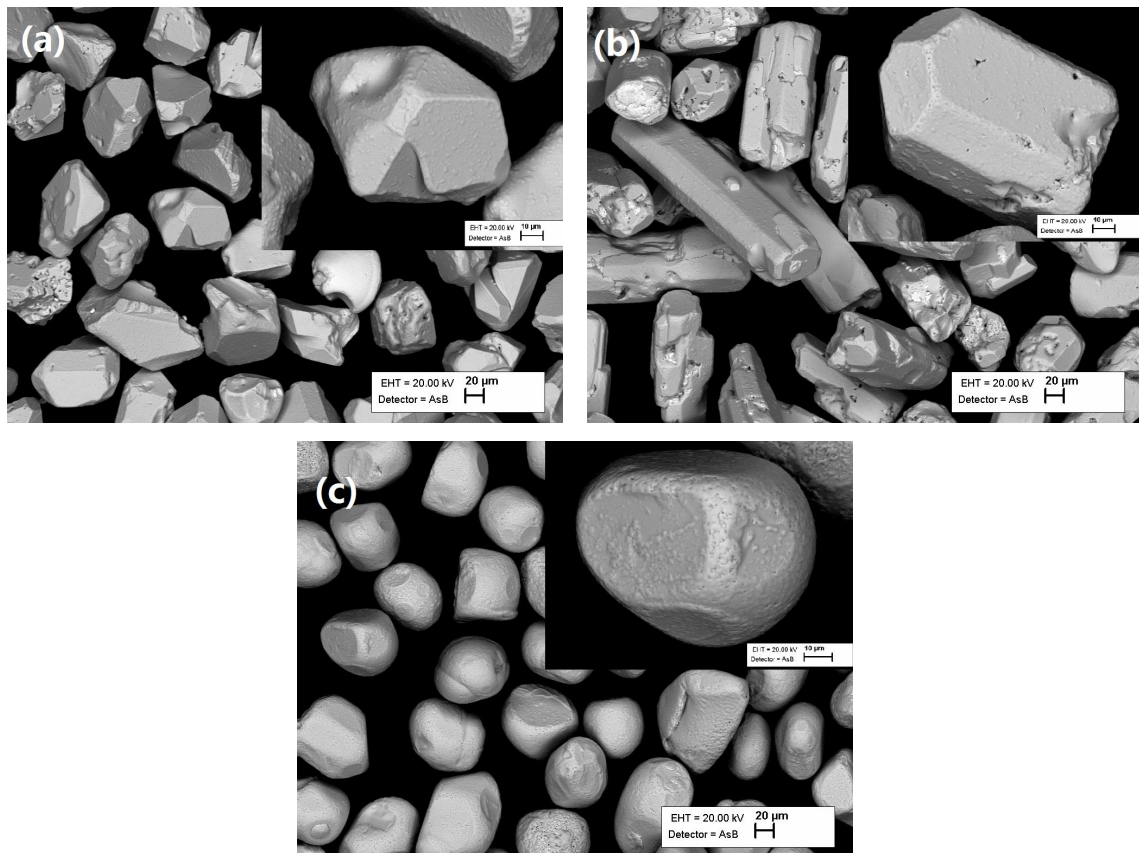


Figure 3.4 The SEM images of $\text{Cu}_2\text{CdGeSe}_4$ monograin powders (fraction 63-75 μm) synthesized in CdI_2 at temperatures a) 500 $^\circ\text{C}$ (Powder 1), b) 600 $^\circ\text{C}$ (Powder 2) and c) 700 $^\circ\text{C}$ (Powder 3).

Monograins synthesized at 500 °C with CdI₂ flux material (Figure 3.4 (a)) had distinguished less rounded edges of grain. In the Figure 3.4 (b) is shown the monograins formed at 600 °C in CdI₂ flux material. The grains have not round shape, the surfaces are rough and more irregularities and small holes on the surfaces have appeared. With the increasing synthesis temperature, the formation processes are accelerated. The solubility of powders is higher than low temperature condition as well.

In the Figure 3.5, it is shown the SEM images of Cu₂CdGeSe₄ powder crystals grown in two different fluxes - KI and CdI₂ at the same synthesis temperature 700 °C. SEM micrograph (Figure 3.5 (a)) shows that monograins synthesized at 700 °C for 120 hours in CdI₂ flux material have rounded edges and the plain surfaces are smooth. Moreover, sintering and holes also can be detected. Figure 3.5 (b) shows the monograins synthesized in the KI flux material at 700 °C. It does not show big difference for the shape of powders between the two different flux conditions.

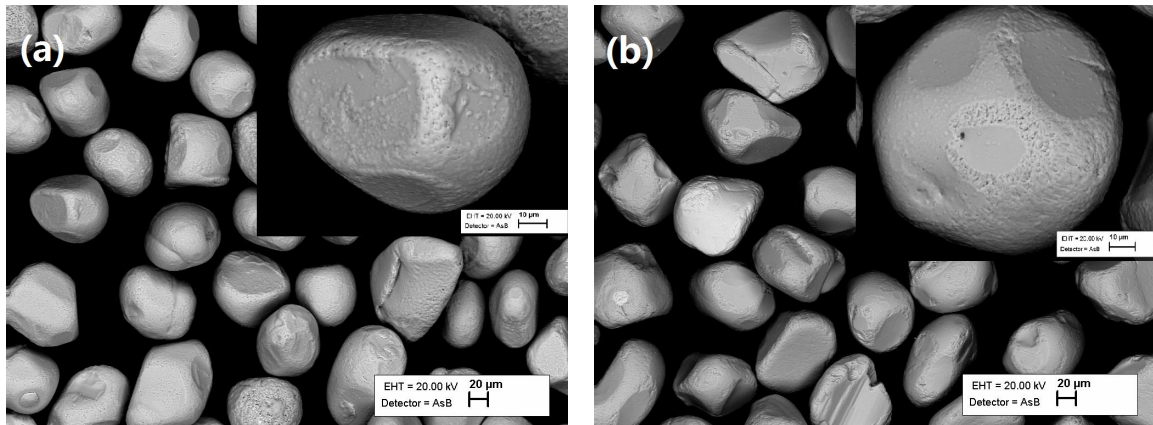


Figure 3.5 The SEM images of Cu₂CdGeSe₄ monograin powders (fraction 63-75 µm) synthesised at temperature 700 °C a) in CdI₂ flux (Powder 3), b) in KI flux (Powder 4).

Figure 3.6 presents the SEM images of Cu₂CdGeSe₄ powder crystals grown in molten KI at the same synthesis temperature 700 °C but different synthesis time. Figure 3.6 (a) shows that the monograins synthesised in KI flux material at 700 °C for 60 hours have rounded edges. Also some holes and irregularities reveal in this condition. Figure 3.6 (b) shows that the monograins had the same shape with very rounded edges already after 120 hours of synthesis time. It does not show big difference in the shape of powders by using 60 or 120 hours of synthesis time, but the median size of powder crystals increased about 20 µm by increasing the synthesis time from 60 hours to 120 hours.

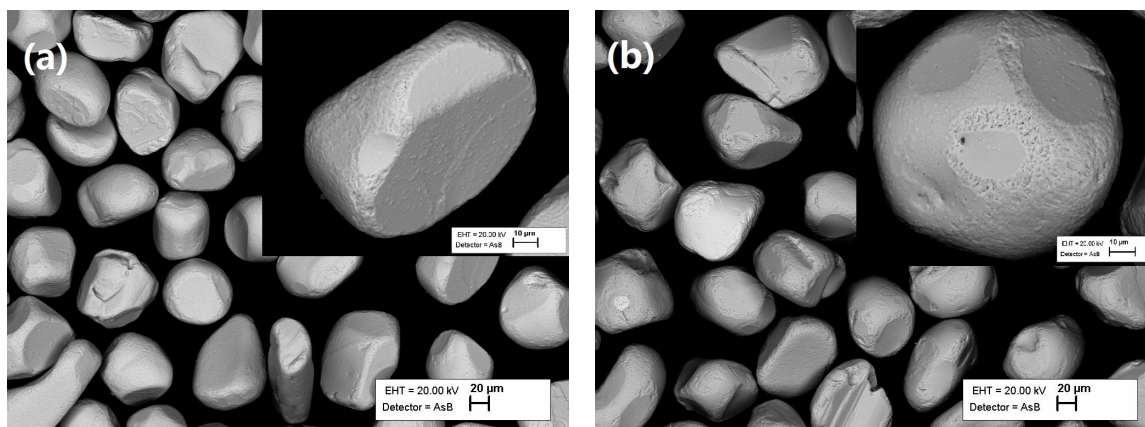


Figure 3.6 The SEM images of $\text{Cu}_2\text{CdGeSe}_4$ monograin powders (fraction 63-75 μm) synthesized at temperature 700 $^\circ\text{C}$, in KI for a) 60 hours (Powder 5) and b) 120 hours (Powder 4).

3.2.2.1 Influence of chemical etching on the crystal surface morphology

In Figure 3.7 the influence of chemical etching to the surface morphology of monograins is presented. In Figure 3.7 (a) is shown the SEM micrographs of the monograin powders before chemical etching (10 % KCN + 1 % KOH). The crystals have slightly smooth edges and small precipitates on the surface. After chemical etching with 10 % KCN + 1 % KOH solution, the grains are more rounded and deeper holes revealed on the edges of powders (Figure 3.7 (b)). Moreover, some smooth crystal planes are revealed.

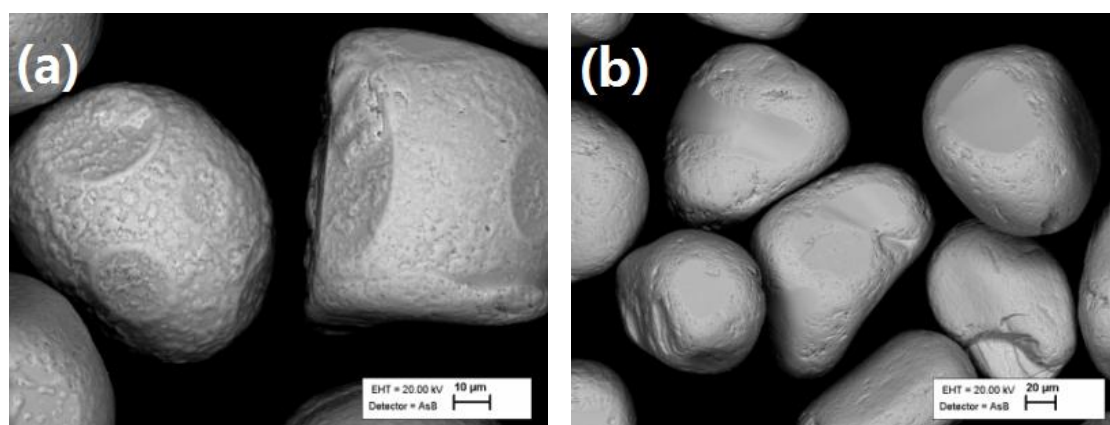


Figure 3.7 The SEM images of $\text{Cu}_2\text{CdGeSe}_4$ monograin powders a) before and b) after chemical etching with 10 % KCN+1 % KOH solution.

3.3 Elemental composition of $\text{Cu}_2\text{CdGeSe}_4$ monograin powders

Bulk composition of the $\text{Cu}_2\text{CdGeSe}_4$ powders synthesized in CdI_2 and KI flux at different temperature was characterized by EDX. Figure 3.8 shows the atomic concentrations of elements in the CdI_2 synthesized powders. The content of Cu and Se remain almost the same atomic

concentrations with increasing synthesis temperature, while the atomic concentrations of Cd increases and Ge decreases, respectively. Increasing the synthesis temperature from 500 °C to 700 °C, the bulk composition becomes Cd-rich (the ratio of $[Cd]/[Ge]$ increases from 0.99 to 1.07). The ratio of $[Cu]/([Cd]+[Ge]) \sim 1.0$ for $Cu_2CdGeSe_4$ powders synthesized in CdI_2 at 500 °C and 700 °C, but powders synthesized at 600 °C have Cu-poor (the ratio of $[Cu]/([Cd]+[Ge]) = 0.93$) and Cd-rich composition.

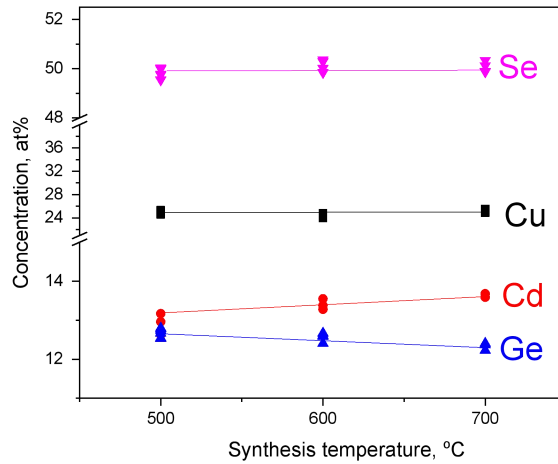


Figure 3.8 Atomic concentration of elements in the powders synthesized in CdI_2 flux at different temperatures.

Bulk composition of the $Cu_2CdGeSe_4$ powders synthesized in KI flux for different times was Cd-rich (the ratio of $[Cd]/[Ge] = 1.03$) and did not depend on synthesis time. But the ratio of $[Cu]/([Cd]+[Ge])$ decreased from 1.0 to 0.96 by increasing synthesis time.

In the Table 3.6 is presented the surface and bulk composition of $Cu_2CdGeSe_4$ monograin powders synthesized in CdI_2 and KI flux at 700 °C. Surface composition of both powders are Cu-rich ($[Cu]/([Cd]+[Ge]) > 1$) and the ratio of $[Cd]/[Ge]$ is close to 1. Bulk composition of powder synthesized in CdI_2 is more Cd-rich ($[Cd]/[Ge] = 1.07$) than the bulk composition of powder synthesized in KI ($[Cd]/[Ge] = 1.02$).

Table 3.6 Composition of $Cu_2CdGeSe_4$ monograin powders synthesized in KI and CdI_2 flux at 700 °C

Material		Cu, at%	Cd, at%	Ge, at%	Se, at%	$[Cu]/([Cd]+[Ge])$	$[Cd]/[Ge]$
Powder 3 700 °C - CdI_2	surface	26.3	11.8	12.0	49.9	1.10	0.98
	bulk	25.4	12.9	12.0	49.7	1.02	1.07
Powder 4 700 °C - KI	surface	26.3	12.1	12.0	49.5	1.09	1.01
	bulk	24.6	12.9	12.7	49.8	0.96	1.02

3.4 Phase composition of $\text{Cu}_2\text{CdGeSe}_4$ monograin powders

3.4.1 XRD analysis

Figure 3.9 shows the XRD patterns of the $\text{Cu}_2\text{CdGeSe}_4$ powders synthesized in CdI_2 flux at different temperature. The powder X-ray diffraction pattern of the powder synthesized at 500 °C showed a tetragonal crystal structure with the space group $I-42m$ of the main phase and addition to the main phase – CdSe. The powders synthesized at 600 °C and 700 °C revealed the presence of an orthorhombic phase and additional CdSe secondary phase. The strongest diffraction peaks are indexed as corresponding to the (112) and (024) planes of tetragonal phase of $\text{Cu}_2\text{CdGeSe}_4$ (PDF- 2/Release 2013 RDB, 01-070-9042). Major diffraction peaks are indexed as (210), (020) and (312) for orthorhombic phase of $\text{Cu}_2\text{CdGeSe}_4$ (PDF-2/Release 2013 RDB, 01-074-3115). Lattice parameters a, b, c of all the samples were calculated and presented in the Table 3.7.

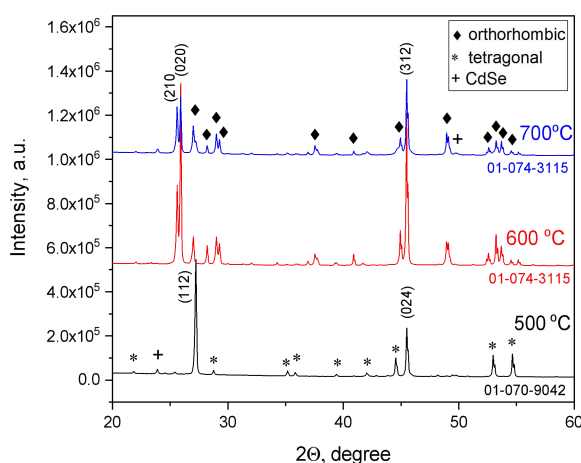


Figure 3.9 X-ray diffraction patterns of $\text{Cu}_2\text{CdGeSe}_4$ powder synthesised in CdI_2 flux at: (a) 500 °C; (b) 600 °C and (c) 700 °C.

Table 3.7 Lattice parameters of $\text{Cu}_2\text{CdGeSe}_4$ monograins

Materials	Space group	a, Å	b, Å	c, Å
Powder 1 (500 °C)	I-42m-tetrag.	5.7476	5.7476	11.0511
Powder 2 (600 °C)	Pmn21-ortor.	8.0726	6.8855	6.6118
Powder 3 (700 °C)	Pmn21-ortor.	8.0634	6.8793	6.6035

3.4.2 Raman analysis

Raman spectroscopy was used to confirm the phase composition of $\text{Cu}_2\text{CdGeSe}_4$ monograins grown at different temperatures. The Raman spectra were recorded to all of the monograin powders grown in different synthesis conditions. In the Figure 3.10 and 3.11, red and black lines show the Raman spectra of $\text{Cu}_2\text{CdGeSe}_4$ powders before and after chemical etching, respectively.

Figure 3.10 demonstrates Raman spectra of HT-Cu₂CdGeSe₄ with orthorhombic structure; while Raman spectra of LT-Cu₂CdGeSe₄ with tetragonal structure was showed in the Figure 3.11. Unfortunately there is no Raman data for this compound in the literature. The main Raman modes for the orthorhombic Cu₂CdGeSe₄ phase (HT-Cu₂CdGeSe₄) were detected at 162, 187, 203, 271 and 277 cm⁻¹ (Figure 3.10), and for tetragonal Cu₂CdGeSe₄ phase (LT-Cu₂CdGeSe₄), the main peaks were at 175, 203, 263 and 292 cm⁻¹ (Figure 3.11).

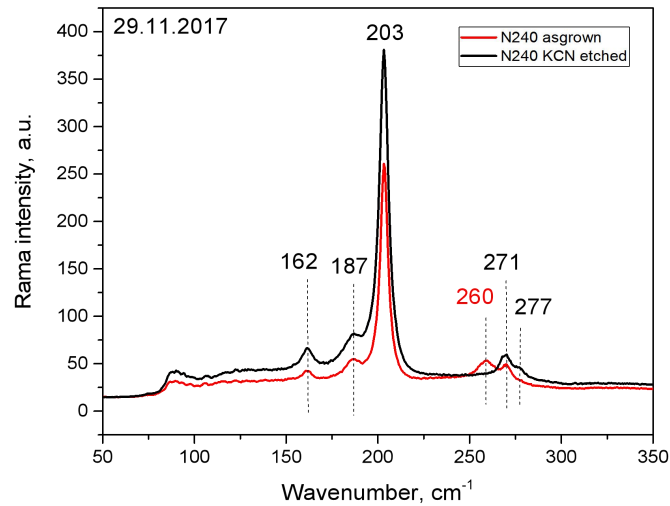


Figure 3.10 RT Raman spectra of Cu₂CdGeSe₄ with orthorhombic structure (powder synthesised at 700 °C in CdI₂ flux, before and after KCN etching).

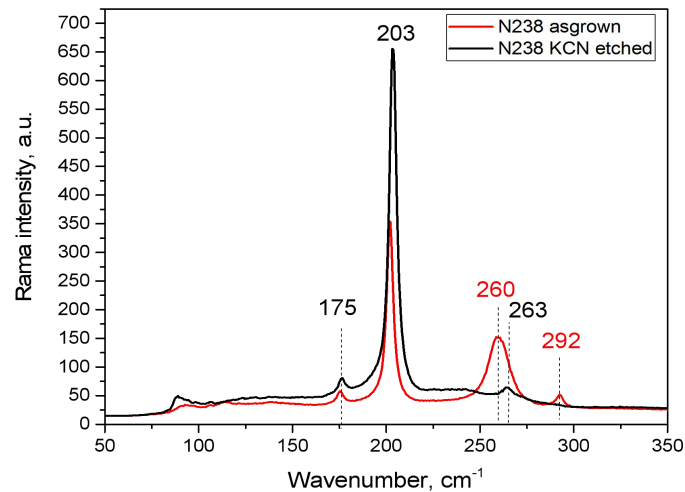


Figure 3.11 RT Raman spectra of Cu₂CdGeSe₄ with tetragonal structure (powder synthesised at 500 °C in CdI₂ flux, before and after KCN etching).

All asgrown powders had additional peak at 260 cm⁻¹, which is assign to Cu₂Se phase [65]. Cu₂Se is known as a semimetallic material. The KCN etching is used for the selective removal of Cu-rich phases. The Raman spectra (Figure 3.10, 3.11) show that the binary phase of Cu₂Se is removed after chemical etching with 10 % KCN + 1 % KOH solution.

3.5 Electrical properties of $\text{Cu}_2\text{CdGeSe}_4$ monograin powders

Measurement of grain resistance require the crystals size at least $100\ \mu\text{m}$. Therefore, the powder crystals synthesized at $500\ ^\circ\text{C}$ were left out as size of the grains was too small (see section 3.1). For grain resistance measurements, 15 grains of size fraction $200 - 224\ \mu\text{m}$ were selected from each powder. The dependence of resistance of the $\text{Cu}_2\text{CdGeSe}_4$ powder crystals on the composition is shown in Figure 3.12. All monograin powders exhibited p-type conductivity regardless of the ratio of $[\text{Cu}]/([\text{Cd}]+[\text{Ge}])$.

The powder crystals have a high conductivity, if the ratio of $[\text{Cu}]/([\text{Cd}]+[\text{Ge}])$ is over one (Cu-rich). The resistance of grains increases, if the ratio of $[\text{Cu}]/([\text{Cd}]+[\text{Ge}]) < 1$ (Cu-poor), which is more suitable for powders as absorbers to manufacture solar cells. According to these results, the powder 4 with the Cu-poor and Cd-rich composition was selected for the monograin layer solar cell preparation and characterisations.

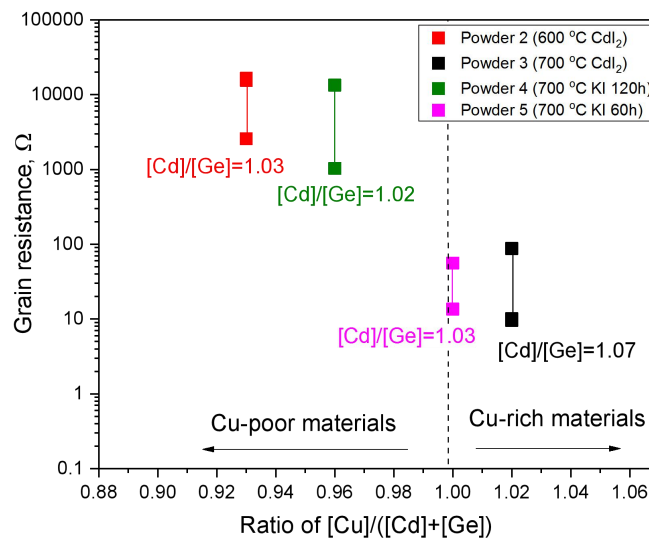


Figure 3.12 The grain resistance of $\text{Cu}_2\text{CdGeSe}_4$ monograins according to concentration ratio of $[\text{Cu}]/([\text{Cd}]+[\text{Ge}])$.

3.6 Device characterization

$\text{Cu}_2\text{CdGeSe}_4$ monograin powder (Powder 4) was used as absorber material in monograin layer solar cells with superstrate structure: graphite/MGL- $\text{Cu}_2\text{CdGeSe}_4$ /CdS/ZnO/glass. Before making the monograin layer membrane, the $\text{Cu}_2\text{CdGeSe}_4$ powder (Powder 4) was post-treated isothermally at elevated temperature as described in Section 2.1.1. Figure 3.13 (a) shows the illuminated IV-curves of MGL solar cells prepared from the powders with LT- and HT- $\text{Cu}_2\text{CdGeSe}_4$ modifications. The black line shows the IV-characteristic of MGL solar cell based on

LT-Cu₂CdGeSe₄ powder and the blue line shows IV-curve of MGL solar cell based on HT-Cu₂CdGeSe₄ powder. For the device based on LT-Cu₂CdGeSe₄ absorber, the obtained power conversion efficiency (PCE) was 2.16 % with open circuit voltage (V_{oc}) of 315 mV, short circuit current (J_{sc}) of 14.7 mA/cm², and fill factor (FF) of 35 %. While for the HT-Cu₂CdGeSe₄ solar cell, a PCE of 4.21 % was achieved, with a V_{oc} of 464 mV, J_{sc} of 17.5 mA/cm² and FF of 39 %.

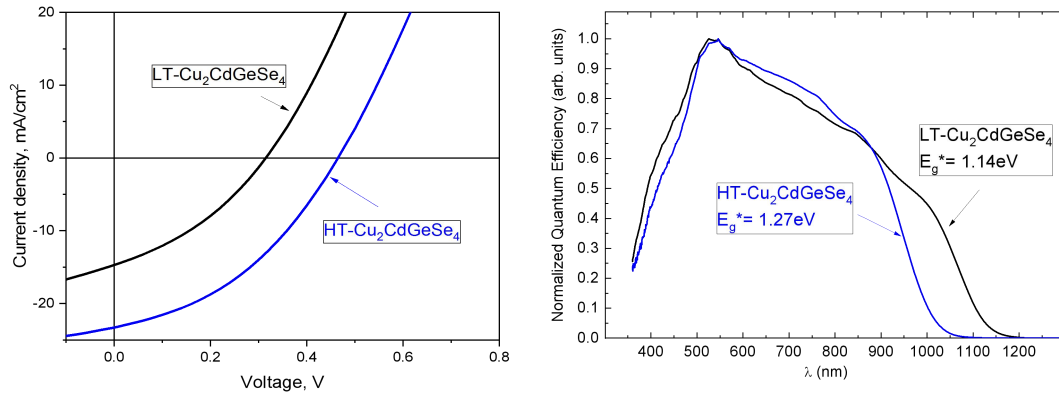


Figure 3.13 a) IV-characteristics and b) EQE spectra of MGL solar cell prepared from LT- and HT-Cu₂CdGeSe₄ powders.

Table 3.8 Data of main characteristics of MGL solar cell prepared from LT- and HT-Cu₂CdGeSe₄ powders

Sample	V_{oc} , mV	J_{sc} , mA/cm ²	FF, %	Eff, %	Active area, mm ²
LT-Cu ₂ CdGeSe ₄	315	19.6	35	2.16	285
HT-Cu ₂ CdGeSe ₄	464	23.3	39	4.21	2.63

The evaluation of E_g from the UV-VIS-NIR reflectance spectra of monograins is rather challenging. EQE analysis is an alternative method that can be used to estimate the effective bandgap energy E_g^* of the synthesized absorber materials [65]. The EQE of Cu₂CdGeSe₄ solar cells was measured as a function of the wavelength of the incident light at room temperature (see Figure 3.13 (b)). The normalized EQE spectra of MGL solar cells show a shift of the absorption edge to shorter wavelength. The E_g^* values calculated from EQE measurements were 1.27 eV for orthorhombic structured powders and 1.14 eV for tetragonal structured powders.

SUMMARY

The quaternary $\text{Cu}_2\text{CdGeSe}_4$ has suitable properties for photovoltaic applications - p-type conductivity, high absorption coefficient ($> 10^4 \text{ cm}^{-1}$) and direct energy band gap (1.2 - 1.29 eV). However, the formation conditions and properties of $\text{Cu}_2\text{CdGeSe}_4$ monograin powders have not been studied.

In this thesis, new quaternary compound $\text{Cu}_2\text{CdGeSe}_4$ was synthesized by molten salt method for photovoltaic applications. $\text{Cu}_2\text{CdGeSe}_4$ powder materials were synthesized from binary compounds (CuSe, CdSe) and elemental metal powder (Ge) and Se at temperatures - 500, 600, and 700 °C in the liquid phase of KI and CdI_2 as the flux materials. The effect of salt material (CdI_2 and KI), synthesis temperature and synthesis time on the structural, morphological, compositional and optoelectronic properties was investigated.

The sieving analysis revealed that median particle size of produced powder crystals increased with increasing synthesis temperature and duration. Median sizes of particles are 25, 58 and 139 μm for powders synthesized in CdI_2 at 500, 600 and 700 °C, respectively. Median sizes of particles are 112 and 132 μm for powders synthesized in KI flux for 60 and 120 hours, respectively.

Structural analysis by Raman spectroscopy and X-ray diffraction showed that $\text{Cu}_2\text{CdGeSe}_4$ powder synthesized at 500 °C had a tetragonal structure and powders synthesized at temperatures 600 and 700 °C had orthorhombic structure.

Compositional analysis by EDX showed that increasing the synthesis temperature from 500 to 700 °C, the bulk composition becomes Cd-rich. The powders synthesized in CdI_2 at 500 and 700 °C had stoichiometric composition ($[\text{Cu}]/([\text{Cd}]+[\text{Ge}]) \sim 1.0$), but powders synthesized at 600 °C had Cu-poor composition ($[\text{Cu}]/([\text{Cd}]+[\text{Ge}]) = 0.93$). Bulk composition of the $\text{Cu}_2\text{CdGeSe}_4$ powders synthesized in KI flux for different times was Cd-rich and did not depend on synthesis time, but the ratio of $[\text{Cu}]/([\text{Cd}]+[\text{Ge}])$ decreased from 1.0 to 0.96 by increasing synthesis time.

All monograin powders exhibited p-type conductivity regardless of the composition, but powders with Cu-poor and Cd-rich compositions were produced at 600 °C in CdI_2 or 700 °C in KI flux.

The band gap obtained from EQE measurements was found to be 1.27 eV for orthorhombic structured powders and 1.14 eV for tetragonal structured powders. The best solar cell fabricated from the HT- $\text{Cu}_2\text{CdGeSe}_4$ powder showed the power conversion efficiency of 4.21 % (active area), with an open-circuit voltage of 0.46 V, a short-circuit current density of 23.3 mA/cm^2 and fill factor of 39 %.

LIST OF REFERENCES

- [1] S. Aldous, How solar cells work. How Stuff Works, 2000.
- [2] P. Jackson, D. Hariskos, R. Wuerz, O. Kiowski, A. Bauer, T. M. Friedlmeier, M. Powalla, Phys. Status Solidi (RRL) 9, 28-31 (2015). <https://doi.org/10.1002/pssr.201409520>.
- [3] W. Wang, M. T. Winkler, O. Gunawan, T. Gokmen, T. K. Todorov, Y. Zhu, D. B. Mitzi, Adv. Energy Mater. 4, (2014) 1301465. <https://doi.org/10.1002/aenm.201301465>.
- [4] G. E. Davidiyuk, O. V. Parasyuk, S. A. Semenyuk et al. Inorganic Materials 39 (2003) 919.
- [5] S. Chen, A. Walsh, Y. Luo, J. Yang, X. G. Gong, S. Wei Phys. Rev.B, 82 (2010), p.195203.
- [6] Renewable Energy Policy Network for the 21st century (REN21), Renewables 2010 Global Status Report, Paris, 2010, pp. 1–80.
- [7] T. Hunt, "The Solar Singularity Is Nigh", Greentech Media, 2015.
- [8] K. Zweibel, Basic photovoltaic principles and methods. Van Nostrand Reinhold, 1984.
- [9] R. L. Bailey, Solar-electrics research and developments, Arbor Science Publishers, Inc., 1980.
- [10] M. S. Sarma, Introduction to Electrical Engineering, Oxford University Press, N.Y, 2001.
- [11] J. Chu, Development of Photovoltaic Solar Cell Technology, AAPPS Bulletin, 2012, 22(4).
- [12] M. A. Green, Third generation photovoltaics: Ultra-high conversion efficiency at low cost. Progress in Photovoltaics Research & Applications 9 (2), (2001), 123-135. <https://doi.org/10.1002/pip.360>
- [13] T L. Floyd, Electronic Devices (Conventional Current Version) (8th Edition) Person International Edition, 2008.
- [14] <http://www.semiconductorforu.com/pn-junction-formed>
- [15] <http://www.pveducation.org/pvcdrom/solar-cell-structure>
- [16] V. V. Tyagi, N. A. A. Rahim, N. A. Rahim et al. Progress in solar PV technology: Research and achievement, Renewable & Sustainable Energy Reviews 20(4), (2013) 443-461. <https://doi.org/10.1016/j.rser.2012.09.028>
- [17] I. Klavina, T. Kaljuvee, K. Timmo et al. Study of Cu₂ZnSnSe₄ monograin formation in molten KI starting from binary chalcogenides, Thin Solid Films 519(21), (2011) 7399-7402. <https://doi.org/10.1016/j.tsf.2011.01.365>
- [18] K. Yoshikawa, H. Kawasaki, W. Yoshida et al. Silicon heterojunction solar cell with interdigitated back contacts for a photoconversion efficiency over 26 %. Nat Energy 2 (5), (2017) 17032.
- [19] B. M. Kayes, H. Nie, R. Twist, S. G. Spruytte, F. Reinhardt, I. C. Kizilyalli, G. S. Higashi, 27.6 % conversion efficiency, a new record for single-junction solar cells under 1 sun illumination, Proceedings of the 37th IEEE Photovoltaic Specialists Conference, 2011.
- [20] M. Wanlass, Systems and methods for advanced ultra-high-performance InP solar cells, US Patent 9, 590, 131 B2, 7 March 2017.
- [21] S. Kim, S. T. Hwang, W. Yoon, H. M. Lee, High performance GaAs solar cell using heterojunction emitter and its further improvement by ELO technique. Paper 4CV.1.27, European Photovoltaic Solar Energy Conference, 2016.

- [22] T. Kato, A. Handa, T. Yagioka, et al. Enhanced efficiency of Cd-free Cu(In,Ga)(Se,S)₂ minimodule via (Zn,Mg)O second buffer layer and alkali post treatment. *IEEE J. of Photovolt.* Vol. 7 (6) (2017) 1773– 1780. <https://doi.org/10.1109/jphotov.2017.2745710>
- [23] First Solar press release: <http://investor.firstsolar.com/news-releases/news-release-details/first-solar-achieves-yet-another-cell-conversion-efficiency>, 24 February 2016.
- [24] W. Wang, M. T. Winkler, O. Gunawan et al. Device characteristics of CZTSSe thin-film solar cells with 12.6 % efficiency, *Adv. Energy Mater.* 4, (2014) 1301465. <https://doi.org/10.1002/aenm.201301465>
- [25] T. Ibn-Mohammed, S. C. L. Koh, I. M. Reaney et al., Perovskite solar cells: An integrated hybrid lifecycle assessment and review in comparison with other photovoltaic technologies, *Renewable & Sustainable Energy Reviews* 80, (2017) 1321-1344. <https://doi.org/10.1016/j.rser.2017.05.095>
- [26] M. A. Green, K. Emery, Y. Hishikawa et al. Solar cell efficiency tables (version 49), *Prog. Photovolt: Res. Appl.* 25 (2017) 333– 334. <https://doi.org/10.1002/pip.2876>
- [27] A. Goodrich, P. Hacke, Q. Wang et al. A wafer-based monocrystalline silicon photovoltaics road map: Utilizing known technology improvement opportunities for further reductions in manufacturing costs, *Solar Energy Materials & Solar Cells* 114 (7) (2013) 110-135. <https://doi.org/10.1016/j.solmat.2013.01.030>
- [28] J. A. Kilner, S. J. Skinner, S. J. C. Irvine et al. *Functional Materials for Sustainable Energy Applications*, Woodhead Publishing, 2014.
- [29] Y. Zhou, *Eco- and Renewable Energy Materials*, Science Press, 2013.
- [30] D. Derkacs, S. H. Lim, P. Matheu et al., Improved performance of amorphous silicon solar cells via scattering from surface plasmon polaritons in nearby metallic nanoparticles, *Applied Physics Letters* 89 (9) (2006) 514-518. <https://doi.org/10.1063/1.2336629>
- [31] A. Luan, D. Smith, P. Cousin et al. Leakage pathway layer for solar cell: US, US9202960[P]. 2015.
- [32] M. A. Green, K. Emery, Y. Hishikawa, W. Warta, E. D. Dunlop, *Solar Cell Efficiency Tables (Version 45)*, *Prog. Photovolt: Res. Appl.* 23 (2015) 1-9. <https://doi.org/10.1002/pip.2573>
- [33] R. W. Miles, *Photovoltaic solar cells: Choice of materials and production methods*, *Vacuum* 80 (10) (2006) 1090-1097. <https://doi.org/10.1016/j.vacuum.2006.01.006>
- [34] B. A. Andersson, *Materials availability for large-scale thin-film photovoltaics*, *Prog. Photovolt. Res. Appl.* 8(1) (2000) 61- 76. [https://doi.org/10.1002/\(SICI\)1099-159X\(200001/02\)8:1<61::AID-PIP301>3.0.CO;2-6](https://doi.org/10.1002/(SICI)1099-159X(200001/02)8:1<61::AID-PIP301>3.0.CO;2-6).
- [35] S. A. Mkrtchyan, K. Dovletov, E. G. Zhukov, A.G Melikdzhanyan, S. Nuryev, *Neorg. Mater.* 24 (1988) p. 1094
- [36] H. Matsushita, T. Maeda, A. Katsui, T. Takizawa, Thermal analysis and synthesis from the melts of Cu-based quaternary compounds Cu-III-IV-VI₄ and Cu₂-II-IV-VI₄ (II=Zn, Cd; III=Ga, In; IV=Ge, Sn; VI=Se), *Journal of Crystal Growth* 208 (2000) 416- 422. [https://doi.org/10.1016/S0022-0248\(99\)00468-6](https://doi.org/10.1016/S0022-0248(99)00468-6)
- [37] H. Matsushita, T. Ichikawa, A. Katsui, Structural, thermodynamical and optical properties of Cu₂-II-IV-VI₄ quaternary compounds, *J Mater Sci* 40 (2005) 2003-2005. <https://doi.org/10.1007/s10853-005-1223-5>

- [38] L. D. Gulay, Ya. E. Romanyuk, O. V. Parasyuk, Crystal structures of low- and high-temperature modifications of $\text{Cu}_2\text{CdGeSe}_4$, *J. Alloys Compd.* 347 (2002) 193–197. [https://doi.org/10.1016/S0925-8388\(02\)00790-9](https://doi.org/10.1016/S0925-8388(02)00790-9)
- [39] R. Chetty, J. Dadda, J. de Boor, E. Müller, R. C. Mallik, The effect of Cu addition on the thermoelectric properties of $\text{Cu}_2\text{CdGeSe}_4$, *Intermetallics* 57 (2015) 156–162. <https://doi.org/10.1016/j.intermet.2014.10.015>
- [40] E. Quinteroa, R. Tovar, M. Quinteroa, G. E. Delgado et al., Lattice parameter values and phase transitions for the $\text{Cu}_2\text{Cd}_{1-z}\text{Mn}_z\text{SnSe}_4$ and $\text{Cu}_2\text{Cd}_{1-z}\text{Fe}_z\text{SnSe}_4$ alloys, *Journal of Alloys & Compounds* 432, Issues 1–2 (2007) 142–148. <https://doi.org/10.1016/j.jallcom.2006.05.126>
- [41] M. G. Brik, O. V. Parasyuk, G. L. Myronchuk, I. V. Kityk, Specific features of band structure and optical anisotropy of $\text{Cu}_2\text{CdGeSe}_4$ quaternary compounds, *Mater. Chem. Phys.* 147 (2014) 155–161. <https://doi.org/10.1016/j.matchemphys.2014.04.022>
- [42] V. A. Ocheretova, O. V. Parasyuk, A. O. Fedorchuk, O. Y. Khyzhun, Electronic structure of $\text{Cu}_2\text{CdGeSe}_4$ single crystal as determined from X-ray spectroscopy data, *Materials Chemistry and Physics* 160 (2015) 345–351. <https://doi.org/10.1016/j.matchemphys.2015.04.049>
- [43] L. V. Piskach, O. V. Parasyuk, Ya. E. Romanyuk. The phase equilibria in the quasi-binary $\text{Cu}_2\text{GeS}_3/\text{Se}_3\text{–CdS/Se}$ systems, *Journal of Alloys & Compounds* 299 (1–2) (2000) 227–231. [https://doi.org/10.1016/S0925-8388\(99\)00797-5](https://doi.org/10.1016/S0925-8388(99)00797-5)
- [44] J. Krustok, T. Raadik; R. Kaupmees; M. Grossberg; M. Kauk-Kuusik; K. Timmo; A. Mere, Observation of band gap fluctuations and carrier localization in $\text{Cu}_2\text{CdGeSe}_4$, *Materials Science and Engineering B*, (2018) publication is under review.
- [45] I. D. Olekseyuk, L. V. Piskach, O. V. Parasyuk O. M. Mel'nyk, T. ALyskovetz, *Journal of Alloys and Compounds* 298(1–2) (2000) 203–212, [https://doi.org/10.1016/S0925-8388\(99\)00669-6](https://doi.org/10.1016/S0925-8388(99)00669-6)
- [46] O. F. Zmiy, I. A. Mishchenko, I. D. Olekseyuk, Phase equilibria in the quasi-ternary system $\text{Cu}_2\text{Se–CdSe–In}_2\text{Se}_3$, *Journal of Alloys & Compounds* 367 (1–2) (2004) 49–57. <https://doi.org/10.1016/j.jallcom.2003.08.011>
- [47] C. Carcaly, N. Chézeau, J. Rivet, J. Flahaut, Description du système $\text{GeSe}_2\text{–Cu}_2\text{Se}$. Transition de phases du composé Cu_8GeSe_6 (Description of the System $\text{GeSe}_2\text{–Cu}_2\text{Se}$. Phase Transition in Cu_8GeSe_6), *Bull. Soc. Chim. Fr.* 4, (1973) 1191–1195, in French
- [48] D. Li, F. Ling, Z. Zhu et al. Theoretical studies on the structural, electronic, and optical properties of $\text{Cu}_2\text{CdGeSe}_4$, *Physica B Condensed Matter* 406 (12) (2011) 3299–3302. <https://doi.org/10.1016/j.physb.2011.05.044>
- [49] A. Luque, S. Hegedus, *Handbook of Photovoltaic Science and Engineering*, 2nd Edition, 2011.
- [50] I. Klavina, J. Raudoja, M. Altosaar et al. CZTS ($\text{Cu}_2\text{ZnSnSe}_4$) crystal growth for use in monograin membrane solar cells, *Conference proceedings of the Conference of Young Scientists on Energy Issues* (2010) VII 345–VII 353.
- [51] E. Mellikov, M. Altosaar, M. Kauk-Kuusik et al., Growth of CZTS-Based Monograins and Their Application to Membrane Solar Cells // *Copper Zinc Tin Sulfide-Based Thin-Film Solar Cells*, John Wiley & Sons Ltd, (2015) 289–309.
- [52] M. Altosaar, A. Jagomägi, M. Kauk, M. Krunks et al., Monograin layer solar cells, *Thin Solid Films* 431–432(1) (2003) 466–469. [https://doi.org/10.1016/S0040-6090\(03\)00167-6](https://doi.org/10.1016/S0040-6090(03)00167-6).
- [53] Growth of Chalcopyrite Single Crystals in *Material Science and Technology: Encyclopedia of Materials: Science and Technology*, 1131–1136.

- [54] R. Boistelle, J. P. Astier, Crystallization mechanisms in solution, *Journal of Crystal Growth* 90(1-3) (1988) 14-30. [https://doi.org/10.1016/0022-0248\(88\)90294-1](https://doi.org/10.1016/0022-0248(88)90294-1).
- [55] R. H. Arendt, The Molten Salt Synthesis of Single Magnetic Domain BaFe₁₂O₁₉ Crystals, *Journal of Solid State Chemistry* 8(4) (1973) 339-347.
- [56] D. H. Kerridge, Recent advances in molten salts as reaction media, *Book of Fourth International Conference on Non-Aqueous Solutions* (1975) 355-371.
- [57] Y. V. Kokunov, Y. E. Gorbunova, G. A. Razgonyaeva et al., Synthesis, crystal structures, and luminescence spectra of the coordination compounds of cadmium(II) iodide with hexamethylenetetramine, *Russian Journal of Coordination Chemistry* 38(10) (2012) 657-661.
- [58] H. Kaur, Points to Ponder in the Study of Cadmium Iodide, *International Letters of Chemistry, Physics and Astronomy* 8 (2014) 1-5.
- [59] M. Danilson, doctoral thesis "Temperature Dependent Electrical Properties of Kesterite Monograin Layer Solar Cells" (2016) Tallinn University of Technology, Estonia.
- [60] R. C. Lord, Introduction to Infrared and Raman Spectroscopy, *Journal of the American Chemical Society* 87(5) (1990) 1155-1156.
- [61] O. Volobujeva. Doctoral thesis "SEM study of selenization of different thin metallic films" (2008) Tallinn University of Technology, Estonia.
- [62] S. H. Aharinejad, A. Lametschwandtner, *Fundamentals of Scanning Electron Microscopy, Microvascular Corrosion Casting in Scanning Electron Microscopy* (1992) 44-51
- [63] J. Goldstein, D. E. Newbury, P. Echlin et al. *Scanning electron microscopy and X-ray microanalysis: a text for biologists, materials scientists, and geologists*, Springer Science & Business Media, 2012.
- [64] J. Krustok, R. Josepson, T. Raadik et al. Potential fluctuations in Cu₂ZnSnSe₄ solar cells studied by temperature dependence of quantum efficiency curves, *Physica B Condensed Matter* 405(15) (2010) 3186-3189. <https://doi.org/10.1016/j.physb.2010.04.041>.
- [65] T. Tanaka, T. Sueishi, K. Saito, Q. Guo, M. Nishio, K. M. Yu, W. Walukiewicz, Existence and removal of Cu₂Se second phase in coevaporated Cu₂ZnSnSe₄ thin films, *Journal of Applied Physics* 111 (2012) 053522. doi: 10.1063/1.3691964.

APPENDIX

Manuscript of the paper in titled “Study of $\text{Cu}_2\text{CdGeSe}_4$ monograin powders synthesized by molten salt method for photovoltaic applications”

M. Kauk-Kuusik, X. Li, M. Pilvet, K. Timmo, M. Grossberg, T. Raadik, M. Danilson, V. Mikli, M. Altosaar, J. Krustok, J. Raudoja

Results will be presented in the EMRS Spring Conference 2018 and published in *Thin Solid Films* 2018